Investigating the assimilation of CALIPSO global aerosol vertical observations using Four-Dimensional Ensemble Kalman Filter

Yueming Cheng[1,2], Tie Dai[1,2*], Daisuke Goto[3], Nick A. J. Schutgens[4], Guangyu Shi[1,2], and Teruyuki Nakajima[5]

5 [1]Collaborative Innovation Center on Forecast and Evaluation of Meteorological Disasters, Nanjing University of Information Science and Technology, Nanjing, China
[2]State Key Laboratory of Numerical Modeling for Atmospheric Sciences and Geophysical Fluid Dynamics, Institute of Atmospheric Physics, Chinese Academy of Sciences, Beijing, China
[3]National Institute for Environmental Studies, Tsukuba, Japan
10 [4]Faculty of Science, Free University of Amsterdam, Amsterdam, Netherlands
[5]Earth Observation Research Center, Japan Aerospace Exploration Agency, Tsukuba, Japan

Corresponding author: Tie Dai (daitie@mail.iap.ac.cn)

Abstract. The aerosol vertical information is critical to quantify the influences of the aerosol on the climate and environment, however large uncertainties still persist in model simulations. In this study, the vertical aerosol extinction coefficients from
15 Cloud-Aerosol Lidar with Orthogonal Polarization (CALIOP) onboard Cloud–Aerosol Lidar and Infrared Pathfinder Satellite Observation (CALIPSO) are assimilated to optimize the hourly aerosol fields of the Non-hydrostatic ICosahedral Atmospheric Model (NICAM) online coupled with the Spectral Radiation Transport Model for Aerosol Species (SPRINTARS) using the four-dimensional Local Ensemble Transform Kalman Filter (4D-LETKF). Additionally, a parallel assimilation experiment using the bias-corrected Aerosol Optical Thicknesses (AOTs) from the Moderate Resolution
20 Imaging Spectroradiometer (MODIS) is conducted to investigate the effects of assimilating the observations whether including the vertical information on the model performances. The assimilation experiments are successfully performed for a one-month long, making it possible to evaluate the results in a statistical sense. The hourly analyses are validated via both the CALIOP observed aerosol vertical extinction coefficients and the AOT observations from the MODIS and AErosol RObotic NETwork (AERONET). Our results reveal both the CALIOP and MODIS assimilations can improve the model
25 simulations. The CALIOP assimilation is superior to the MODIS assimilation in modifying the incorrect aerosol vertical distributions and reproducing the real magnitudes and variations. However, the MODIS assimilation can better reproduce the AOT distributions than the CALIOP assimilation. This is probably due to the nadir-viewing CALIOP has much sparser coverages than the MODIS. The assimilation efficiencies of CALIOP decrease with the increasing distances of the overpass time, indicating that more aerosol vertical observation platforms are required to fill the sensor-specific observation gaps and
30 hence improve the aerosol vertical data assimilation.

1 Introduction

Aerosols have significant impacts on the air quality, climate change, radiation balance, and hydrological cycle (Charlson et al., 1992; Nakajima et al., 2001; Huang et al., 2014; Ramanathan et al., 2001). Aerosols may also contribute to the regional

35 differences in the historical warming rates (Huang et al., 2017). Due to the large uncertainties in the parameterizations of the various aerosol processes such as emission, transport, and deposition, it is still a challenge for model itself to accurately quantify the effects of aerosols on the earth system (Huneeus et al., 2011; Myhre et al., 2013; Textor et al., 2006; Sato et al., 2018; Sato and Suzuki, 2019). Aerosol data assimilation, which makes optimal use of both observations and numerical simulations to obtain the best possible estimates of aerosol behaviors, is an emerging way for getting accurate predictions

40 and characterizations of atmospheric aerosol and its influence.

Recently, aerosol assimilation studies have been conducted to improve the model simulation performances generally using one of the optimal interpolation, variational, and ensemble-based methods. The assimilated aerosol observations commonly include the space-borne or ground-based aerosol optical thicknesses (AOTs) from the POLDER (Generoso et al., 2007), MODIS (Dai et al., 2014; Di Tomaso et al., 2017; Hyer et al., 2011; Liu et al., 2011; Yin et al., 2016a, 2016b; Yumimoto et

45 al., 2011; Yumimoto et al., 2017; Zhang and Reid, 2006), Himawari-8 (Dai et al., 2019; Yumimoto et al., 2018), AERONET (Schutgens et al., 2010a, 2010b), and the multi-sensor (Rubin et al., 2017; Zhang et al., 2014). Although assimilating AOTs can strongly constrain the horizontal distributions of the aerosol burdens, there are limited in improving the vertical information of aerosols. The vertical distribution of aerosols is a combined characteristic of atmospheric transport patterns, residence times in the atmosphere and the efficiency of the vertical energy exchange (Koffi et al., 2012; Yu et al., 2010),

50 which shows the large diversities up to an order of magnitude among models (Textor et al., 2006). Reductions of the large uncertainties in the aerosol vertical distributions are of crucial importance for the accurate evaluation of the aerosol impacts on the earth system such as the aerosol direct effect (Oikawa et al., 2013, 2018).

Apart from the AOTs, the aerosol vertical information such as the aerosol extinction coefficient is another variable for aerosol assimilation. Uno et al. (2008) and Yumimoto et al. (2008) developed a four-dimensional variational (4D-Var)

55 assimilation system with a regional dust model to assimilate the retrieved-extinction coefficient from the ground-based NIES Lidar network for investigating Asian dust. Due to the limited spatio-temporal frequencies of the aerosol vertical observations and the noise signal from the lidar observations, the aerosol vertical assimilation is still at an initial stage. The Cloud–Aerosol Lidar and Infrared Pathfinder Satellite Observation (CALIPSO), which carried the Cloud-Aerosol Lidar with Orthogonal Polarization (CALIOP) instrument with high horizontal and vertical resolutions, exhibits great potential for

60 reducing the uncertainties in the global spatio-temporal distributions of aerosols especially the vertical profiles in the aerosol transport models. A coupled 2D/3D-Var system which assimilated the CALIOP-retrieved aerosol extinction profiles for two weeks was developed by Zhang et al. (2011). Zhang et al. (2014) also conducted the multi-sensor experiments and found that the inclusion of CALIOP data can improve the aerosol vertical distribution and hence forecasted advection. The variational data assimilation systems use the pre-calculated static model error covariance matrix, whereas the ensemble-based Kalman

65 filter (EnKF) can generate a flow-dependent model error covariance matrix to better represent the background error (Evensen, 1994). The flow-dependent model errors are calculated by the ensemble simulations. Sekiyama et al. (2010) initially applied the four-dimensional Local Ensemble Transform Kalman filter (4D-LETKF) to assimilate the CALIOP attenuated backscattering coefficients with the analysis at the center of the 48 h assimilation window. However, the hourly aerosol analyses using the 4D-LETKF approach can provide more accurate aerosol features for investigating the

70 environmental and climate effects of aerosols (Dai et al., 2019).

Therefore, in the present study, we apply the 4D-LETKF and an aerosol model named Spectral Radiation Transport Model for Aerosol Species (SPRINTARS) online coupled with a new dynamical atmospheric model called Non-hydrostatic ICosahedral Atmosphere Model (NICAM) to generate hourly aerosol horizontal and vertical analyses for one-month using the CALIOP aerosol extinctions. The results are validated using both the CALIOP extinctions and the MODIS and

75 AERONET AOTs observations. To the best of our knowledge, this is probably the first study to conduct the hourly aerosol vertical extinctions assimilation using four-dimensional ensemble Kalman method for one month.

The observation data used in this study are described in Sect. 2. The forward model and the data assimilation methodology are described in Sect. 3. Section 4 presents the assimilation results and their validations. The discussions and the main conclusions achieved in this study are shown in Sect. 5 and Sect. 6, respectively.

80 2 Observational Data

2.1 CALIOP

CALIOP, a space-borne two-wavelength polarization lidar that is the prime payload instrument carried by the CALIPSO satellite, probes the high-resolution vertical structures and properties of clouds and aerosols since 2006 (Winker et al., 2007). CALIPSO flies as one of 5 satellites in the so-called "A-train" constellation of satellites, and all the satellites are in the 705

85 km sun-synchronous polar orbit with a 16-day repeat cycle. During both day and night, the CALIOP continuously provides vertical profiles of aerosol extinction coefficient at 532 nm and 1064 nm, with a uniform spatial resolution of 60 m vertically and 5 km horizontally over an altitude range of -0.5 km to 30 km. In this study, we only use the aerosol extinction coefficients at 532 nm in the CALIPSO lidar level 2 (L2) Version 4.10 aerosol profile products over the altitude range below 10 km (http://www-calipso.larc.nasa.gov/).

90 2.2 MODIS

The Moderate Resolution Imaging Spectroradiometer (MODIS) aboard both NASA's Terra and Aqua satellites is making near-global daily observations of the earth in a wide spectral range (0.41-15 μm) (Remer et al., 2005). In this study, the MODIS-Aqua Collection 6.1 level 2 Dark Target (DT)/Deep Blue (DB) merged AOT observations at 550 nm are used to validate the model simulations. The DT and DB merged AOT provides a more gap-filled dataset than the observation which

95 is only retrieved from the individual algorithms (https://modis.gsfc.nasa.gov) (Levy et al., 2013; Sayer et al., 2014). The

Community Intercomparison Suite (CIS) tool (Watson-Parris et al., 2016), which was developed to allow the straightforward comparison of remote sensing, in situ and model data, is used to aggregate the level 2 MODIS AOTs at 10 km and 5 minutes resolution to produce the hourly MODIS AOTs at 2°×2°for comparison.

2.3 AERONET

100 The AErosol RObotic NETwork (AERONET; http://aeronet.gsfc.nasa.gov/) Version 3 (V3) data provides globally distributed near-real-time observations of aerosol spectral optical thickness at nominal standard aerosol wavelengths as 340, 380, 440, 500, 675, 870, 1020, and 1640 nm (Holben et al., 1998; Giles et al., 2019). Due to the both availability of the AOTs at 440 nm in most AERONET sites and the model calculations, we directly use the level 2 cloud-screened AERONET AOTs at 440 nm for the validation. The AERONET retrieved instantaneous AOTs within the preceding 1h are averaged to

105 calculate the hourly mean AOTs for comparison.

3 Model and Data Assimilation Methodology

3.1 Model

A global three-dimensional aerosol transport model SPRINTARS (Takemura et al., 2000; Takemura et al., 2003; Takemura et al., 2009) online coupled with NICAM (Satoh et al., 2005; Satoh et al., 2008; Satoh et al., 2014; Tomita and Satoh., 2004)

110 is used as the forward model to predict the aerosol spatial and temporal evolutions. The major tropospheric aerosols including dust, sea salt, sulfate, and carbonaceous aerosols are simulated in NICAM-SPRINTARS considering the main aerosol processes including emissions, advection, dry and wet depositions. A three-dimensional icosahedral grid advection scheme preserving monotonicity and consistency with continuity for aerosol transport is adopted in NICAM (Niwa et al., 2011). The dust and sea salt aerosols spanning wide size ranges are divided into 10 and 4 bins for transport, respectively,

115 whereas the sulfate and carbonaceous aerosols are predicted using the bulk modal method (Takemura et al., 2000). The aerosol-cloud-radiation interactions are included in the aerosol-coupled version of NICAM (Sato et al., 2018). In this study, the NICAM-SPRINTARS is set up with a homogeneous horizontal resolution about 223 km and a vertical resolution of 40 layers from surface to approximately 40 km altitude. The vertical grid spaces approximately 160 m near the surface, and the spaces exponentially increase to approximately 1320 m around 16 km. NICAM is successfully applied to produce a high-

120 resolution global simulation with a horizontal resolution of about 0.87 km (Miyamoto et al., 2013), indicating a potential application of a sub-kilometer global aerosol simulation and data assimilation when the computer resources are available. With the stretched-grid system, NICAM can also be used to run by partially high resolution simulations in the object regions (Goto et al., 2015). Therefore, there is a future prospect to extend the present assimilation method to fine scale regional analyses using the stretched-grid system implemented in NICAM (Uchida et al., 2016, 2017). The biomass burning and

125 anthropogenic emission inventories for BC, OC, and SO_2 used in this study are from the Global Fire Emissions Database

(GFEDv3.1; van der Werf et al., 2010) and the Hemispheric Transport of Air Pollution (HTAP; Janssens-Maenhout et al., 2015) as same as in Dai et al. (2019). The dust and sea salt emission fluxes are both mainly depended on the near-surface wind speeds (Dai et al., 2018; Takemura et al., 2009). The meteorological fields in NICAM are nudged by the reanalysis data every 6 h from the NCEP Final (FNL) Analysis (https://rda.ucar.edu/datasets/ds083.2/) to reduce the influences of the

130   uncertainties in the meteorological conditions on the aerosol simulations.

3.2 Data Assimilation Methodology

The 4D-LETKF (Dai et al., 2019; Hunt et al., 2007) assimilation system of the NICAM_SRPINTARS is used to assimilate the CALIOP vertical extinction observations, which is an extension of the LETKF to assimilate the asynchronous observations. One advantage of the 4D-LETKF is the localization technique, which allows the local analyses to choose

135   different linear combinations of the ensemble members in local regions using a prescribed localization scale to explore a much higher-dimensional space than the ensemble space and reduce the spurious correlations with distance (Hunt et al., 2007). Furthermore, localization enables parallel computation to reduce computational cost (Yumimoto et al., 2018). The horizontal and vertical localization are both performed in the observational error covariance matrix by the physical distance to avoid discontinuity in the analysis (Miyoshi et al., 2007). The observational error covariance matrix is calculated as the

140   observation uncertainties multiple the inverse of the horizontal and the vertical localization factors, that the effect of observation on analysis is descending by the distance increasing. The horizontal and vertical localization factors are both defined following Gaussian shapes as $exp(-r^2/2\sigma^2)$, where the σ represents the localization length and the r is the distance of observations from the local patch center. Although the Gaussian function has infinitely long tails, we truncate the tails to simulate the fifth-order piecewise rational function by Gaspari and Cohn (1999), which is widely used localization

145   weighting function in the EnKF studies (Miyoshi et al., 2007). The fifth-order rational function drops to zero at $r = 2 \cdot \sqrt{10/3} \cdot \sigma$ and we do not assimilation observations beyond this distance.

A total of 668 CALIPSO orbit paths over November 2016 are obtained and used for the aerosol data assimilation. To identify the aerosol signals and screen out the cloud signals, we applied several quality control procedures to remove the noisy or highly uncertain observations before aggregating the profile data. The quality controls include (1) the vertical

150   feature mask must be determined as aerosols; (2) the Cloud-Aerosol Discrimination (CAD) score must be lower than -80, indicating high confidence of discriminating as aerosols; (3) Extinction Quality Control (QC) flag must be equal to 0 or 1 (Young and Vaughan, 2009); (4) the extinction coefficient must be greater than 0 and less than 100 km $^{-1}$; (5) the uncertainty of extinction coefficient must be lower than 10 km $^{-1}$, indicating the stable iteration.

After the quality control of the data, we aggregate the original CALIOP extinction coefficients to the model grid boxes.

155   Firstly, we perform the hourly horizontal aggregation to the model horizontal resolution about 2°×2° in the CALIOP observations level (i.e., every 0.06 km) using the mean value of all the reasonable sub-grid observations within ±30 minutes. The CALIOP extinction observations within the range of $\mu \pm \sigma$ are used for the average, where μ and σ represent the mean

and the standard deviation of the sub-grid observations in the aggregation cell respectively. To avoid assimilation of sub-grid features likely to create anomalous feature in the horizontal 2° grid cell (Schutgens et al., 2017), the number of the used retrievals within 2° grid cell must be also greater than 20 and the coefficient of extinction variations within the grid cell (i.e., standard deviation/mean) must be less than 0.5 as similar as Zhang and Reid. (2006). Then, the horizontally regridded observations within each model layer are averaged to serve as the assimilated observations. The observation uncertainties are assumed to be 20% of the mean aerosol extinctions in reference to Winker et al. (2007) and Sekiyama et al. (2010).

We apply the 4D-LETKF data assimilation system to the global aerosol vertical analysis of November 2016. Data assimilation is initiated at 00:00 UTC on 1 November 2016 and terminated at 00:00 UTC on 1 December 2016. The initial condition at 00:00 UTC on 1 November are prepared by a one-month simulation which is executed by NICAM-SPRINTARS without any aerosol data assimilation as a spin-up. The assimilation time window is 24 hours for the 4D-LETKF, and the modeled aerosol fine and coarse mass mixing ratios are hourly optimized using the hourly aggregated observations during the assimilation window (Dai et al., 2019). A single deterministic simulation with the default model configuration is performed as a reference (a free running, FR experiment hereafter). Two data assimilation experiments are performed to investigate the effects of assimilating the observations whether including the vertical information on the model simulations. The first one assimilates the CALIPSO vertical extinction coefficients (DA-CALIPSO experiment hereafter). In the second one, the U.S. Naval Research Laboratory (NRL) quality-assured and controlled MODIS Level-3 gridded AOTs are assimilated (DA-NRL experiment hereafter). The NRL AOTs including no vertical information have been subjected to extensive quality assurance and quality check procedures for aerosol assimilation (Hyer et al., 2011; Zhang and Reid, 2006). The assimilation system parameters are based on several tuning experiments as discussed in Sect. 5. Twenty members with spatiotemporally perturbing aerosol emissions are used to generate the model ensemble simulations. The perturbation factors follow lognormal distributions as same as those used in Dai et al. (2019), except the uncertainty of sea salt is assumed as 500% following Yumimoto and Takemura (2011). This is due to the emission fluxes of sea salt are still not well known, which can span a factor about 20 for the different source functions even excluding outliers (Grythe et al., 2014). The horizontal and vertical localization lengths are set as 200 km and one model layer (increasing by the altitude), respectively. To prevent filter divergence, the multiplicative inflation with a fixed factor of 1.1 is performed on the background ensemble following Sekiyama et al. (2010).

4 Results

The results in the FR, DA-NRL, and DA-CALIPSO experiments are compared and verified with the assimilated CALIOP vertical extinctions and the AOT observations obtained from the MODIS and AERONET. To quantify the model performances, the statistical criteria (Boylan and Russell, 2006; Willmott et al., 2012; Yumimoto et al., 2017), including the mean fractional bias (MFB), the mean fractional error (MFE), the root mean square error (RMSE), the correlation coefficient (CORR) and the index of agreement (IOA), are calculated between the simulated results and observations. Because of the

190   small differences between the AOTs at 532 nm and 550 nm, i.e., between 2% and 4% for typical Angstrom exponents of 0.5 to 1 (Kittaka et al., 2011), we directly use the modeled aerosol extinction coefficients at 550 nm to compared with the CALIOP observations at 532 nm.

4.1 Comparison of the Analysis With CALIOP

The CALIOP analysis performances are firstly evaluated with the assimilated CALIOP extinction coefficients at 532 nm as
195   sanity or internal checks (Benedetti et al., 2009), which can directly illustrate the benefits of assimilating the CALIOP vertical observation on the model simulations. Figures 1a-f show the scatter plots of the assimilated CALIOP extinction coefficients versus the simulated ones over the global land and ocean, and Figures 1g-h further show the probability distribution functions (PDFs) of collocated forecast-minus-observation deviations in the FR experiment and analysis-minus-observation deviations in the DA-NRL and DA-CALIPSO experiments. Based on the model performance evaluation
200   statistical metrics (i.e., MFB, MFE, RMSE, CORR, and IOA), the DA-NRL experiment is slightly superior to the FR experiment, whereas the DA-CALIPSO experiment is evidently better than the FR experiment especially over the ocean regions. The CORR values are 0.317 and 0.365 over the global land and ocean for the FR experiment, whereas the DA-CALIPSO experiment significantly improves the CORRs to 0.668 and 0.782 respectively. Compared to the FR experiment, the scatters between the simulated and observed extinction coefficients over both the global land and ocean are more
205   concentrated, and more points align with the 1:1 line for the CALIOP assimilation. The distributions of the extinction coefficient deviations in the FR experiment show the systematically negative biases, indicating the model tends to underestimate the extinction coefficients in most of the world. The distributions over the ocean in the DA-NRL experiment are slightly superior to those in the FR experiment, whereas the probabilities of the deviations within ±0.01(±0.02) over the land are even lower than those in the FR experiment. This indicates the AOT assimilation has a limited improvement of the
210   aerosol vertical distribution, although the AOT simulation can be improved (see Fig. 7). Obviously, the PDFs over both the land and ocean in the DA-CALIPSO experiment are symmetrical to the value of 0 and more squeezed with higher peaking. Merely 13.56% (27.49%) and 15.73% (32.03%) of the extinction coefficient deviations over the land and ocean are within ±0.01(±0.02) in the FR experiment, while 36.37% (54.50%) and 49.87% (72.79%) of the deviations are achieved within ±0.01(±0.02) in the DA-CALIPSO experiment. The eliminations of the strong underestimations over both the global land
215   and ocean in the DA-CALIPSO experiment prove that the CALIOP assimilation exhibits obviously improved consistency with the aerosol extinction observations and hence provide a positive sanity check of the assimilation system.

To further assess the benefit of assimilating CALIOP aerosol extinctions and MODIS AOTs on the model simulations over different aerosol regimes, we choose thirteen regions and classify them into four groups according to their surface aerosol emissions regimes (Huang et al., 2013). The column integrated aerosol extinctions from 0 to 10 km altitude is used for
220   comparison. The four groups are dominated by the biomass burning smoke, dust, industrial pollution, and marine aerosols, respectively (Fig. 2a). As shown in Figs. 2b-d, the modeled column integrated extinctions for the three experiments are compared with the CALIOP ones over the thirteen selected regions. All the five statistical metrics of the two assimilation

experiments (DA-CALIPSO and DA-NRL) are superior to those of the FR experiment except the MFB in the DA-NRL experiment, indicating that the spatio-temporal distributions of the column integrated aerosol characteristics can be better

225   reproduced both with the CALIOP and MODIS assimilation. The modeled column integrated extinctions in the FR experiment show the negative biases compared to CALIOP for 11 out of the 13 regions, reaching up to 42% and 66% for the SEA and SAM regions in the biomass burning regime, respectively. With the CALIOP assimilation, the modeled column integrated extinctions are generally increased over all the underestimated regions, leading to the reductions of the absolute bias for 9 out of the 13 regions and all the simulated column integrated extinctions are within a factor of 2 of the observed

230   ones. The RMSE value decreases from 0.028 to 0.022, and the CORR value increases from 0.871 in FR experiment to 0.963 in the DA-CALIPSO assimilation experiment. In addition to the evaluation of the modeled mean column integrated extinctions in Figs. 2b-d, we further employ the Taylor graph (Taylor, 2001) to quantitatively assess the pattern correspondence between the simulated and observed fields on the regional level (Fig. 2e). The correlation coefficient, the centered pattern root mean square (RMS) difference, and the ratios of the modeled and observed standard deviation are all

235   indicated by a single point on a two-dimensional plot. The ratios of the modeled and observed standard deviation in the FR experiment range from the 0.30 over the SAM region to 2.05 over the ECN region, while the upper bounds are significantly down to 1.24 and 1.19 in the DA-NRL and DA-CALIPSO experiments. The regions with obviously underestimated dispersion are less improved by the aerosol data assimilation as shown by the relative small variations of the lower bounds. This is due to the aerosol extinctions are generally strongly underestimated over the regions with underestimated dispersion,

240   making it difficult to generate enough model errors by perturbing aerosol emissions. Thus, the observational errors are too large relative to the model errors, which translates to a reduced impact of the observation on the model state. Among all the thirteen regions, the ratios of the modeled and observed standard deviation in the two assimilation experiments are comparable whereas the DA-CALIPSO experiment achieves more higher correlations and lower RMS differences than those with the MODIS assimilation. This indicates that both the MODIS and CALIOP assimilation can modify the amplitude of

245   the extinction variations, while the CALIOP assimilation can also improve the temporal and spatial variations of the aerosol extinctions.

Figures 3-5 show the scatter plots of the modeled and the CALIOP observed hourly extinction coefficients within 0-10 km over the thirteen regions for the FR, DA-NRL, and DA-CALIPSO experiments, respectively. The aerosol extinctions are classified into 4 altitude ranges (0-0.5 km, 0.5-1.0 km, 1.0-2.0 km, and 2.0-10.0 km) to further investigate the effects of the

250   CALIOP and MODIS data assimilations on the aerosol vertical simulations. The statistical metrics of the DA-NRL experiment are slightly superior to those of the FR experiment over the thirteen regions except for the SAF region, whereas the DA-CALIPSO experiment are clearly superior to those of the FR and DA-NRL experiments over all the thirteen regions. The aerosol extinctions in all the altitudes over the SAF region in the DA-NRL experiment are more underestimated than those in the FR experiment. This is probably due to the MODIS retrieved aerosol loadings over the SAF region are lower

255   than the CALIPSO retrievals (Ma et al., 2013). The large negative MFB values reveal the FR experiment tends to underestimate the aerosol extinction coefficients over all the three biomass burning regions especially over the SAM region.

The improvements of the CALIOP assimilation on the simulated extinction coefficients over the SAM region are not so obvious compared to the other two regions. This is probably due to the emission fluxes of biomass burning aerosols over the SAM region are underestimated obviously, leading to an underestimation of the model uncertainty and, hence, the analysis underweights the observations. The extinction coefficients in the free atmosphere (2-10 km) of the DA-CALIPSO experiment are more narrowly distributed along the 1:1 line than those in the boundary layer (0-2 km) for the SAF and SEA regions. The lower extinction coefficients in the higher altitude and the high injections of fire product induce the model uncertainties are relative larger than the observation ones, hence, the analysis underweights the model. Dust is a predominant component of aerosol in the NAF, WCN, and WAU regions, where the main deserts in the world are located in. The improvements of the simulated extinction coefficients by the CALIOP assimilation in the NAF and WAU regions are more obvious than those in the WCN region. The proportions of observations within 1-2 km (2-10 km) for the NAF, WCN, and WAU regions are 37% (11%), 22% (22%), and 24% (14%), respectively. This indicates that the dust aerosols emitted from the desert in West China have the higher possibilities in transporting in the relatively high altitude than those emitted from the desert in North Africa (Ginoux et al., 2001). Therefore, the dust emission in West China will have wider impacts on the downwind areas than that of NAF, leading to a smaller model spread over the dust source regions of WCN and, hence, the analysis underweights the observations. In the WAU region, the significant overestimations of the extinction coefficients over the 1 km in the FR experiment are probably caused by a simulated dust storm (Dai et al. 2019). The DA-CALIPSO experiment more obviously corrects the significant overestimations than the DA-NRL experiment. In the IND, ECN, WEU, and EUS regions, urban and industrial aerosols are the major part of the aerosol loadings (Penning de Vries et al., 2015). The aerosols in this regime especially over ECN mainly exist below 2 km as indicated by the relatively large extinction coefficients. It is apparent that the CALIOP assimilation can significantly improve the model performances of simulated extinction coefficients over all the four anthropogenic aerosol regions. The NWP, NAT, and CAT regions are oceanic regions located downwind of the major dust and industrial pollution sources. Thus, these oceanic regions are substantially influenced by the mixture of ocean emissions, the ship exhaust, and the transported continental emissions (Sorooshian and Duong, 2010). It is apparent the CALIOP assimilation over the maritime downwind regime has the most efficient improvements among the four regimes. A common problem that the analyses generally fail to correct the significantly underestimated extinction coefficients is found over all the four aerosol regimes. This is probably due to the insufficient emissions lead to the underestimated extinctions and model errors, thus the analysis underweights the observation.

The vertical profiles of the monthly and regional averaged aerosol extinctions and the ratios between the modeled and observed standard deviations of the aerosol extinctions for the three experiments and the collocated CALIOP retrievals over the thirteen regions are shown in Fig. 6. We ignore the levels where the number of the available CALIPSO observations is less than 10. With respect to the biomass burning regime, the FR experiment underestimates the aerosol extinction profiles over all the available levels of all the three biomass burning regions. This indicates the biomass burning emissions in November 2016 are probably stronger than those used in this study. The shape of the simulated extinction profile over the SEA region in the FR experiment is generally consistent to the CALIOP observations, whereas the FR experiment fails to

simulate the descending trend of the extinction coefficients over the SAF region. The DA-CALIPSO experiment decreases the negative biases over all the three biomass burning regions and achieves the descending trend of the extinction coefficients over the SAF region. Moreover, the ratios of the simulated and observed standard deviation over the SAF region with the CALIOP assimilation are closer to 1 than those in the FR experiment. Although the MODIS assimilation eliminates

295   the underestimations in some altitudes in the SAM and SEA regions, the aerosol profile in SAF is more underestimated than that in the FR experiment over all the levels due to the inconsistency between the MODIS and CALIOP observations as mentioned above. With respect to the dust regime, it is found both the MODIS and CALIOP assimilations have marginal impacts on the vertical profiles except over the WAU region. The simulated profile of the extinction coefficients in the DA-CALIPSO experiment over the WAU is apparently more comparable to the CALIOP observed one than that in the FR

300   experiment, and the significantly descending trend in the CALIOP observations below 1 km are successfully reproduced in the DA-CALIPSO experiment. The simulated ascending trend of the aerosol extinctions above 2.5 km over the WAU in the FR experiment is corrected by the two assimilation experiments, which is probably due to the elimination of the simulated dust event. There are limited improvements with data assimilation over the WCN region due to the limited observations to be assimilated. For the NAF region, the CALIOP assimilation induces a slightly larger negative bias of the vertical profile than

305   that of the FR experiment. This is due to the assimilation is more efficient to reduce the positive biases than the negative ones. This situation is also found in the IND region. However, the DA-CALIPSO experiment corrects the unexpected descending trend of the extinction coefficients below 0.2 km in the IND region, whereas the DA-NRL experiment can't achieve such corrections. Over the ECN region, it is obvious that the FR experiment significantly overestimates the extinction coefficients below 1 km. This is due to the anthropogenic emission inventories used in this study are based on the

310   year 2010, whereas the anthropogenic emissions over ECN have been significantly reduced due to the national regulations of the anthropogenic emissions. The CALIOP and the MODIS assimilations both successfully eliminate the significant overestimations below 1 km. Over the WEU region, the DA-CALIPSO experiment reproduces the vertical profile of the aerosol extinctions much better than those in the FR and DA-NRL experiments. Over the EUS region, the overestimations of the extinction coefficients over the 1 km (mainly contributed by the sulfate aerosols) are correctly amended by the data

315   assimilation. Over NWP and NAT regions, although the FR experiment simulates totally opposite vertical distributions of extinction coefficients to those of the CALIOP observations, the DA-CALIPSO experiment other than the DA-NRL experiment reproduces the profile of the CALIOP observations successfully. The significant improvements of the aerosol profiles over the maritime downwind regions are due to the sufficient spread of the sea salt emissions below 2 km (figure not shown for brevity).

320   From our results so far, both the CALIOP or MODIS assimilations can improve the magnitude of the simulated aerosol extinctions when the profile in the FR experiment is reasonable, and the CALIOP assimilation is superior to the MODIS assimilation in terms of modifying the incorrect aerosol vertical distributions and reproducing the real magnitudes and variations.

4.2 Validation of the Analysis With MODIS

325 In this section, we perform an independent validation of the simulated hourly AOTs over the whole month for the three experiments through a comparison with the MODIS Aqua Collection 6.1 AOT products. It is notable we only analyze the simulated AOTs with more than 30% variations between the DA-CALIPSO and FR experiments hereafter to eliminate the potential effects of the sparse CALIPSO observations.

Figures 7a-f show the spatial distributions of the biases and RMSEs between the simulated and the MODIS observed AOTs

330 at 550 nm for the three experiments. In Fig. 7g, we also present the PDF plots of the AOT deviations between the simulated hourly AOTs and the MODIS observed ones over the whole month. The two assimilation experiments especially the DA-NRL experiment significantly reduce the positive biases and the associated high RMSEs over East China and Australia. It is expected that the DA-NRL experiment achieves a better agreement with the MODIS AOTs, since the assimilated NRL AOTs in the DA-NRL experiment are based on the MODIS AOTs. As shown in Fig. 8, the improvements of both the two

335 assimilation experiments over East China mostly benefit from the reductions of anthropogenic sulfate, OC and BC aerosols, and the improvements over Australia mostly benefit from the reductions of natural dust aerosols. The AOTs over the ocean areas are generally underestimated in the FR experiment, and the both the two assimilations correctly increase the sea salt aerosols, leading to the lower biases and RMSEs. It is apparent that the two assimilations also improve the model performances over the tropic Atlantic located at the downwind of North Africa. This is mainly caused by the reductions of

340 the transported dust and OC aerosols, indicating the assimilation improves the simulation of the characteristics of aerosol transport from the Africa to Atlantic. The distribution of the AOT deviations relative to the MODIS Aqua observations for the FR experiment is negatively biased because the FR experiment tends to underestimate the AOTs over most of the ocean region. The two assimilation experiments especially the DA-NRL experiment are superior to the FR experiment as indicated by the reduced biases and the peaks closer to 0. The frequencies of AOTs deviation within ±0.05 in the DA-CALIPSO

345 (58.15%) and DA-NRL (64.16%) experiments are higher than the ones in the FR experiment (44.48%).

Interestingly, it is unexpected that the AOTs in the DA-CALIPSO experiment have the larger biases and RMSEs with the MODIS observations over the western part of the Saharan desert compared to the FR experiment, whereas such deterioration is not found in the DA-NRL experiment. The CALIOP (MODIS) assimilation reduces (increases) the dust AOTs over the western part of the Saharan desert. To investigate the possible reason, Figure 9 gives the spatial distributions of the multi-

350 annual mean AOTs at 550 nm for MODIS Aqua, day-time CALIOP, and night-time CALIOP AOTs at 532 nm. The MODIS and the CALIOP AOTs are averaged from the MODIS Aqua level 3 monthly aerosol products with a 1°×1° resolution and CALIPSO Lidar level 3 Version 3.0 monthly mean gridded aerosol profile products at 2°×5° resolution for the cloud-free conditions in November from 2006 to 2016, respectively. As shown in Fig. 9, the CALIOP AOTs are significantly lower than the MODIS AOTs over the western Saharan desert region, indicating that the deterioration of AOTs comparisons with

355 the MODIS by the CALIOP assimilation is probably due to the differences between the CALIOP and MODIS observations in this region. Ma et al. (2013) also mentioned that the CALIPSO AOT is significantly lower than the MODIS AOT over

dust regions especially over the Saharan region. Schuster et al. (2012) found that the relative and absolute biases are probably due to the assumed Lidar ratio for the CALIPSO dust retrieval is too low.

4.3 Independent Validation of the Analysis With AERONET

360 As shown in Figs. 10a-f, we further present the maps of the validation statistical metrics (biases and RMSEs) between the modeled and the AERONET observed AOTs at 440 nm calculated over the whole month at each AERONET stations for the three experiments. The AERONET sites with more than 10 observations during the study period are selected. The bias in the FR experiment indicates that the model tends to underestimate the AOTs over 60% stations in the world but overestimate the AOTs over the polluted industrial regions such as Eastern America, Western Europe, South and East Asia. The strongest

365 biases and highest RMSEs in the FR experiment are both found in the South and East Asia, and this is due to large uncertainties in the temporal and spatial distributions of the anthropogenic aerosol emissions. The two assimilation experiments especially the DA-NRL experiment clearly reduce the biases and RMSEs over the regions such as Eastern America and Western Europe, indicating both the CALIOP and the MODIS assimilations can improve the model performance to better reproduce the aerosol spatial evolutions. We also give the PDF plots of the AOT deviations between

370 the simulated hourly AOTs and the AERONET observed ones for the three experiments. The negatively biased PDF for the FR experiment also reveals that the simulated AOTs are underestimated globally. The biases are improved as the peaks nearer to 0 with both the CALIOP and MODIS assimilations, and the performance of the DA-NRL experiment is better than that of the DA-CALIPSO experiment. The frequency of AOT deviations within ±0.05 (±0.10) increases from 46.25% (65.96%) in the FR experiment to 57.89% (75.90%) in the DA-NRL experiment.

375 Figure 11a shows the detailed comparisons of the temporal evolutions of the hourly AOTs at 440 nm for the three experiments with the AERONET-retrieved ones over the site named Pushan_NU. Compared to the simulated AOTs in the FR experiment, the modeled AOTs in the assimilation experiments are much closer to the AERONET observed ones, especially reducing the significant overestimations of AOTs from 3 to 7 November. The overestimations in the FR experiment are mainly induced by the sulfate productions due to aqueous phase conversion from SO_2. The CALIOP derived

380 vertical aerosol sub-types (Fig. 11i) are dominated by the sea salt and other aerosols, proving the simulated sulfate productions in the FR experiment are incorrect. In fact, there are no CALIOP orbit paths pass the Pushan_NU site, indicating the improvements of the AOTs over 3 to 7 November can benefit from the assimilation of the CALIOP aerosol extinctions nearby the Pushan_NU site. Figures 11b shows the vertical distributions of the aerosol extinctions at 532nm over one CALIOP orbit path near Pushan_NU site around 18:00 UTC on 3 November, and Fig. 11d, f, and h show the corresponding

385 simulated ones of the three experiments. It is apparent that the FR experiment tends to overestimate the aerosol extinctions with the centers located at altitudes of 1-2 km from 33°N and 124°E to 38°N and 126°E, while the DA-CALIPSO rather than the DA-NRL experiment correctly eliminates the unrealistic high extinction coefficients, making both the aerosol extinctions and AOTs more in accordance with the CALIOP and AERONET observations.

5 Discussions

390 CALIPSO provides sparse observations due to the sensor-specific data gaps for a 16-day repeat cycle. To investigate the effects of the CALIPSO sensor gaps on the data assimilation, Fig. 12 shows the assimilation efficiencies (AE), referred to Yumimoto and Takemura (2011), with the MODIS observed AOTs as a function of the CALIOP overpass time. The hourly and daily mean AEs both show decreasing trends as the increasing distances of the assimilation time. The AEs are high close to the overpass time but deteriorate later on. Such a deterioration demonstrates that more intensive vertical observations can
395 improve the aerosol vertical assimilation efficiency and hence advance the studies of the aerosol effects on the climate and environment.

To investigate the effects of the assimilation system parameters (i.e., horizontal localization length, vertical localization length, and uncertainty of dust emission) on the CALIOP assimilation, other three assimilation experiments named DA-CALIPSO-HL, DA-CALIPSO-VL, and DA-CALIPSO-Dust are conducted. The experiments are in the same model
400 configuration as that of the DA-CALIPSO experiment except twice horizontal localization length used in the DA-CALIPSO-HL experiment, four times vertical localization length used in the DA-CALIPSO-VL experiment, and five times assumed dust uncertainty used in the DA-CALIPSO-Dust experiment. Figure 13 shows the frequencies of the AOT deviations between the simulations of the four CALIPSO assimilation experiments and the independent MODIS observations, in addition, the corresponding result of the FR experiment is also shown as a reference. Although the peaks of the AOT
405 deviation distributions in all the assimilation experiments are closer to 0 compared with that in the FR experiment, the frequencies of the AOT deviations within ±0.05 and ±0.10 in the DA-CALIPSO-VL are significantly lower than those of the other assimilation experiments. This indicates that one model layer is a reasonable vertical localization length and a larger one will reduce the assimilation ability. Moreover, the assimilation of aerosol vertical observation is more sensitive to the vertical localization than the horizontal localization and the uncertainties of the dust emissions.

6 Conclusions

Assimilation of aerosol vertical observations can provide more accurate spatio-temporal distributions of aerosol characteristics especially the vertical information, which should advance the studies of the aerosol effects on the earth system. In the present study, we develop the 4D-LETKF assimilation system for the CALIOP vertical extinction observations and successfully present an one-month long hourly aerosol analyses during November 2016. The hourly analyses are validated
415 by the assimilated CALIOP observations and the MODIS and AERONET retrieved AOTs. The effects of assimilating the observations including the vertical information or not on the model performances are also investigated by an additional assimilation experiment using the bias-corrected MODIS AOT observations.

Both the CALIOP and MODIS assimilations can improve the model simulations, and the CALIOP assimilation is superior to the MODIS assimilation in term of modifying the incorrect aerosol vertical distributions to reproduce the real magnitudes
420 and variations. CALIOP assimilation improves the negative biases of aerosol extinctions considerably in global. The

percentages of the aerosol extinction deviations within ±0.02 increase from 27.49% (32.03%) to 54.50% (72.79%) in land (ocean) respectively, indicating the more efficient enhancements in the ocean. The limited improvements of the underestimated analyses over all the four aerosol regimes demonstrate that the assimilation system has the difficulties in correcting the significantly underestimated extinction coefficients which is probably due to the relatively large observational
425 errors compared to the model errors, and then leads to a reduced impact of the observation on the model state.

Compared with the MODIS and AEROENT retrieved AOTs, the assimilation of CALIOP vertical extinction coefficients achieves improved model simulated AOTs over most of the land and ocean regions. However, the MODIS assimilation can reproduce better agreements with the independent AERONET AOTs than the CALIOP assimilation. This is probably due to the CALIOP (with a 16-day repeat cycle) has much sparser coverages than the MODIS and the assimilation efficiencies of
430 CALIOP decreases with the increasing distances of the assimilation time.

The assimilation of the CALIOP extinction observations deteriorates the model performance over the western part of the Sahara desert compared to the MODIS observations. This is due to the inconsistences between the CALIOP and MODIS observations, indicating the assumed lidar ratio which is important for aerosol extinction retrieval still has the uncertainties especially in the dust regions and the data quality needed to be improved for advancing model skill over these regions.

435 The assimilation efficiencies are high close to the overpass time but deteriorate later on. This indicates that more aerosol vertical observation platforms are required to fill the sensor-specific observation gaps for better aerosol vertical data assimilation. In the near future, joint assimilation of the aerosol profile observations from the Earth Cloud Aerosol and Radiation Explorer (EarthCARE) and CALIPSO may further advance our understanding of the atmospheric aerosol vertical characteristics.

440 **Author contributions.** Tie Dai designed the experiments. Yueming Cheng carried out the experiments and conducted the data analysis with contributions from all co-authors. Yueming Cheng prepared the manuscript with help from Tie Dai, Daisuke Goto, Nick A.J. Schutgens, Guangyu Shi, and Teruyuki Nakajima.

Acknowledgments. This study is financially supported by the Strategic Priority Research Program of the Chinese Academy of Sciences (XDA2006010302), the National Key R&D Program of China (2016YFC0202001, 2017YFC0209803), the
445 National Natural Science Funds of China (41571130024, 41605083, 41590875, and 41475031). Some of the authors are supported by the Global Environment Research and Technology Development Fund S-12 of MOEJ, the Japan Aerospace Exploration Agency (JAXA)/Earth Observation Priority Research, and the Grant-in-Aid for Young Scientist A (grant 17H04711) in Japan. The model simulations were performed using the supercomputer resources NIES/NEC SX-ACE and JAXA/JSS2. We are grateful to the relevant researchers who provided the observation data of AERONET
450 (http://www.eorc.jaxa.jp/ptree/index.html) and MODIS (https://modis-atmos.gsfc.nasa.gov/products/aerosol). CALIPSO data were obtained from the NASA Langley Research Center Atmospheric Sciences Data Center (ASDC).

References

Benedetti, A., Morcrette, J.-J., Boucher, O., Dethof, A., Engelen, R. J., Fisher, M., Flentje, H., Huneeus, N., Jones, L., Kaiser, J. W., Kinne, S., Mangold, A., Razinger, M., Simmons, A. J. and Suttie, M.: Aerosol analysis and forecast in the European

455   Centre for Medium-Range Weather Forecasts Integrated Forecast System: 2. Data assimilation, Journal of Geophysical Research, 114(D13), doi:10.1029/2008JD011115, 2009.

Boylan, J. W., and Russell, A. G.: PM and light extinction model performance metrics, goals, and criteria for three-dimensional air quality models, Atmospheric Environment, 40, 4946-4959, http://dx.doi.org/10.1016/j.atmosenv.2005.09.087, 2006.

460   Charlson, R. J., Schwartz, S. E., Hales, J. M., Cess, R. D., Coakley, J. A., Hansen, E. and Hofmann, D. J.: Climate Forcing by Anthropogenic Aerosols, , 255, 9, 1992.

Dai, T., Schutgens, N. A. J., Goto, D., Shi, G. and Nakajima, T.: Improvement of aerosol optical properties modeling over Eastern Asia with MODIS AOD assimilation in a global non-hydrostatic icosahedral aerosol transport model, Environmental Pollution, 195, 319–329, doi:10.1016/j.envpol.2014.06.021, 2014.

465   Dai, T., Cheng, Y., Zhang, P., Shi, G., Sekiguchi, M., Suzuki, K., Goto, D. and Nakajima, T.: Impacts of meteorological nudging on the global dust cycle simulated by NICAM coupled with an aerosol model, Atmospheric Environment, 190, 99–115, doi:10.1016/j.atmosenv.2018.07.016, 2018.

Dai, T., Cheng, Y., Suzuki, K., Goto, D., Kikuchi, M., Schutgens, N. A. J., Yoshida, M., Zhang, P., Husi, L., Shi, G. and Nakajima, T.: Hourly Aerosol Assimilation of Himawari-8 AOT Using the Four-Dimensional Local Ensemble Transform

470   Kalman Filter, Journal of Advances in Modeling Earth Systems, doi:10.1029/2018MS001475, 2019.

Di Tomaso, E., Schutgens, N. A. J., Jorba, O. and Pérez García-Pando, C.: Assimilation of MODIS Dark Target and Deep Blue observations in the dust aerosol component of NMMB-MONARCH version 1.0, Geoscientific Model Development, 10(3), 1107–1129, doi:10.5194/gmd-10-1107-2017, 2017.

Evensen, G.: Sequential data assimilation with a nonlinear quasi-geostrophic model using Monte Carlo methods to forecast

475   error statistics, J. Geophys. Res., 99(C5), 10143, doi:10.1029/94JC00572, 1994.

Gaspari, G. and Cohn, S. E.: Construction of correlation functions in two and three dimensions, Q.J Royal Met. Soc., 125(554), 723–757, doi:10.1002/qj.49712555417, 1999.

Generoso, S., Bréon, F.-M., Chevallier, F., Balkanski, Y., Schulz, M. and Bey, I.: Assimilation of POLDER aerosol optical thickness into the LMDz-INCA model: Implications for the Arctic aerosol burden, Journal of Geophysical Research,

480   112(D2), doi:10.1029/2005JD006954, 2007.

Giles, D. M., Sinyuk, A., Sorokin, M. G., Schafer, J. S., Smirnov, A., Slutsker, I., Eck, T. F., Holben, B. N., Lewis, J. R., Campbell, J. R., Welton, E. J., Korkin, S. V. and Lyapustin, A. I.: Advancements in the Aerosol Robotic Network (AERONET) Version 3 database – automated near-real-time quality control algorithm with improved cloud screening for Sun photometer aerosol optical depth (AOD) measurements, Atmospheric Measurement Techniques, 12(1), 169–209, 485   doi:10.5194/amt-12-169-2019, 2019.

Ginoux, P., Chin, M., Tegen, I., Prospero, J. M., Holben, B., Dubovik, O. and Lin, S.-J.: Sources and distributions of dust aerosols simulated with the GOCART model, Journal of Geophysical Research: Atmospheres, 106(D17), 20255–20273, doi:10.1029/2000JD000053, 2001.

Goto, D., Dai, T., Satoh, M., Tomita, H., Uchida, J., Misawa, S., Inoue, T., Tsuruta, H., Ueda, K., Ng, C. F. S., Takami, A., 490   Sugimoto, N., Shimizu, A., Ohara, T. and Nakajima, T.: Application of a global nonhydrostatic model with a stretched-grid system to regional aerosol simulations around Japan, Geoscientific Model Development, 8(2), 235–259, doi:10.5194/gmd-8-235-2015, 2015.

Grythe, H., Ström, J., Krejci, R., Quinn, P. and Stohl, A.: A review of sea-spray aerosol source functions using a large global set of sea salt aerosol concentration measurements, Atmospheric Chemistry and Physics, 14(3), 1277–1297, 495   doi:10.5194/acp-14-1277-2014, 2014.

Holben, B. N., Eck, T. F., Slutsker, I., Tanré, D., Buis, J. P., Setzer, A., Vermote, E., Reagan, J. A., Kaufman, Y. J., Nakajima, T., Lavenu, F., Jankowiak, I. and Smirnov, A.: AERONET—A Federated Instrument Network and Data Archive for Aerosol Characterization, Remote Sensing of Environment, 66(1), 1–16, doi:10.1016/S0034-4257(98)00031-5, 1998.

Huang, J., Yu, H., Dai, A., Wei, Y. and Kang, L.: Drylands face potential threat under 2 °C global warming target, Nature 500   Clim Change, 7(6), 417–422, doi:10.1038/nclimate3275, 2017.

Huang, L., Jiang, J. H., Tackett, J. L., Su, H. and Fu, R.: Seasonal and diurnal variations of aerosol extinction profile and type distribution from CALIPSO 5-year observations: Journal of Geophysical Research: Atmospheres, 118(10), 4572–4596, doi:10.1002/jgrd.50407, 2013.

Huang, R.-J., Zhang, Y., Bozzetti, C., Ho, K.-F., Cao, J.-J., Han, Y., Daellenbach, K. R., Slowik, J. G., Platt, S. M., 505   Canonaco, F., Zotter, P., Wolf, R., Pieber, S. M., Bruns, E. A., Crippa, M., Ciarelli, G., Piazzalunga, A., Schwikowski, M., Abbaszade, G., Schnelle-Kreis, J., Zimmermann, R., An, Z., Szidat, S., Baltensperger, U., Haddad, I. E. and Prévôt, A. S. H.: High secondary aerosol contribution to particulate pollution during haze events in China, Nature, 514(7521), 218–222, doi:10.1038/nature13774, 2014.

Huneeus, N., Schulz, M., Balkanski, Y., Griesfeller, J., Prospero, J., Kinne, S., Bauer, S., Boucher, O., Chin, M., Dentener, 510   F., Diehl, T., Easter, R., Fillmore, D., Ghan, S., Ginoux, P., Grini, A., Horowitz, L., Koch, D., Krol, M. C., Landing, W., Liu, X., Mahowald, N., Miller, R., Morcrette, J.-J., Myhre, G., Penner, J., Perlwitz, J., Stier, P., Takemura, T. and Zender, C. S.:

Global dust model intercomparison in AeroCom phase I, Atmospheric Chemistry and Physics, 11(15), 7781–7816, doi:10.5194/acp-11-7781-2011, 2011.

Hunt, B. R., Kostelich, E. J. and Szunyogh, I.: Efficient data assimilation for spatiotemporal chaos: A local ensemble transform Kalman filter, Physica D: Nonlinear Phenomena, 230(1–2), 112–126, doi:10.1016/j.physd.2006.11.008, 2007.

Hyer, E. J., Reid, J. S. and Zhang, J.: An over-land aerosol optical depth data set for data assimilation by filtering, correction, and aggregation of MODIS Collection 5 optical depth retrievals, Atmospheric Measurement Techniques, 4(3), 379–408, doi:10.5194/amt-4-379-2011, 2011.

Janssens-Maenhout, G., Crippa, M., Guizzardi, D., Dentener, F., Muntean, M., Pouliot, G., Keating, T., Zhang, Q., Kurokawa, J., Wankmüller, R., Denier van der Gon, H., Kuenen, J. J. P., Klimont, Z., Frost, G., Darras, S., Koffi, B. and Li, M.: HTAP_v2.2: a mosaic of regional and global emission grid maps for 2008 and 2010 to study hemispheric transport of air pollution, Atmospheric Chemistry and Physics, 15(19), 11411–11432, doi:10.5194/acp-15-11411-2015, 2015.

Kittaka, C., Winker, D. M., Vaughan, M. A., Omar, A. and Remer, L. A.: Intercomparison of column aerosol optical depths from CALIPSO and MODIS-Aqua, Atmospheric Measurement Techniques, 4(2), 131–141, doi:10.5194/amt-4-131-2011, 2011.

Koffi, B., Schulz, M., Bréon, F.-M., Griesfeller, J., Winker, D., Balkanski, Y., Bauer, S., Berntsen, T., Chin, M., Collins, W. D., Dentener, F., Diehl, T., Easter, R., Ghan, S., Ginoux, P., Gong, S., Horowitz, L. W., Iversen, T., Kirkevåg, A., Koch, D., Krol, M., Myhre, G., Stier, P. and Takemura, T.: Application of the CALIOP layer product to evaluate the vertical distribution of aerosols estimated by global models: AeroCom phase I results: AEROSOL PROFILES IN GLOBAL MODELS, Journal of Geophysical Research: Atmospheres, 117(D10201), doi:10.1029/2011JD016858, 2012.

Levy, R. C., Mattoo, S., Munchak, L. A., Remer, L. A., Sayer, A. M., Patadia, F. and Hsu, N. C.: The Collection 6 MODIS aerosol products over land and ocean, Atmospheric Measurement Techniques, 6(11), 2989–3034, doi:10.5194/amt-6-2989-2013, 2013.

Liu, Z., Liu, Q., Lin, H.-C., Schwartz, C. S., Lee, Y.-H. and Wang, T.: Three-dimensional variational assimilation of MODIS aerosol optical depth: Implementation and application to a dust storm over East Asia: AOD DATA ASSIMILATION, Journal of Geophysical Research: Atmospheres, 116(D23206), doi:10.1029/2011JD016159, 2011.

Ma, X., Bartlett, K., Harmon, K. and Yu, F.: Comparison of AOD between CALIPSO and MODIS: significant differences over major dust and biomass burning regions, Atmospheric Measurement Techniques, 6(9), 2391–2401, doi:10.5194/amt-6-2391-2013, 2013.

Miyamoto, Y., Kajikawa, Y., Yoshida, R., Yamaura, T., Yashiro, H. and Tomita, H.: Deep moist atmospheric convection in a subkilometer global simulation: CONVECTION IN A SUB-KM GLOBAL SIMULATION, Geophysical Research Letters, 40(18), 4922–4926, doi:10.1002/grl.50944, 2013.

Miyoshi, T., Yamane, S. and Enomoto, T.: Localizing the Error Covariance by Physical Distances within a Local Ensemble Transform Kalman Filter (LETKF), SOLA, 3, 89–92, doi:10.2151/sola.2007-023, 2007.

545   Myhre, G., Samset, B. H., Schulz, M., Balkanski, Y., Bauer, S., Berntsen, T. K., Bian, H., Bellouin, N., Chin, M., Diehl, T., Easter, R. C., Feichter, J., Ghan, S. J., Hauglustaine, D., Iversen, T., Kinne, S., Kirkevåg, A., Lamarque, J.-F., Lin, G., Liu, X., Lund, M. T., Luo, G., Ma, X., van Noije, T., Penner, J. E., Rasch, P. J., Ruiz, A., Seland, Ø., Skeie, R. B., Stier, P., Takemura, T., Tsigaridis, K., Wang, P., Wang, Z., Xu, L., Yu, H., Yu, F., Yoon, J.-H., Zhang, K., Zhang, H. and Zhou, C.: Radiative forcing of the direct aerosol effect from AeroCom Phase II simulations, Atmospheric Chemistry and Physics, 550   13(4), 1853–1877, doi:10.5194/acp-13-1853-2013, 2013.

Nakajima, T., Higurashi, A., Kawamoto, K. and Penner, J. E.: A possible correlation between satellite-derived cloud and aerosol microphysical parameters, Geophysical Research Letters, 28(7), 1171–1174, doi:10.1029/2000GL012186, 2001.

Niwa, Y., Tomita, H., Satoh, M. and Imasu, R.: A Three-Dimensional Icosahedral Grid Advection Scheme Preserving Monotonicity and Consistency with Continuity for Atmospheric Tracer Transport, Journal of the Meteorological Society of 555   Japan, 89(3), 255–268, doi:10.2151/jmsj.2011-306, 2011.

Oikawa, E., Nakajima, T., Inoue, T. and Winker, D.: A study of the shortwave direct aerosol forcing using ESSP/CALIPSO observation and GCM simulation: DARF USING CALIPSO AND GCM, Journal of Geophysical Research: Atmospheres, 118(9), 3687–3708, doi:10.1002/jgrd.50227, 2013.

Oikawa, E., Nakajima, T. and Winker, D.: An Evaluation of the Shortwave Direct Aerosol Radiative Forcing Using CALIOP 560   and MODIS Observations, Journal of Geophysical Research: Atmospheres, 123(2), 1211–1233, doi:10.1002/2017JD027247, 2018.

Penning de Vries, M. J. M., Beirle, S., Hörmann, C., Kaiser, J. W., Stammes, P., Tilstra, L. G., Tuinder, O. N. E. and Wagner, T.: A global aerosol classification algorithm incorporating multiple satellite data sets of aerosol and trace gas abundances, Atmospheric Chemistry and Physics, 15(18), 10597–10618, doi:10.5194/acp-15-10597-2015, 2015.

565   Ramanathan, V.: Aerosols, Climate, and the Hydrological Cycle, Science, 294(5549), 2119–2124, doi:10.1126/science.1064034, 2001.

Remer, L. A., Kaufman, Y. J., Tanré, D., Mattoo, S., Chu, D. A., Martins, J. V., Li, R.-R., Ichoku, C., Levy, R. C., Kleidman, R. G., Eck, T. F., Vermote, E. and Holben, B. N.: The MODIS Aerosol Algorithm, Products, and Validation, Journal of the Atmospheric Sciences, 62(4), 947–973, doi:10.1175/JAS3385.1, 2005.

570   Rubin, J. I., Reid, J. S., Hansen, J. A., Anderson, J. L., Holben, B. N., Xian, P., Westphal, D. L. and Zhang, J.: Assimilation of AERONET and MODIS AOT observations using variational and ensemble data assimilation methods and its impact on aerosol forecasting skill, Journal of Geophysical Research: Atmospheres, 122(9), 4967–4992, doi:10.1002/2016JD026067, 2017.

Sato, Y., Goto, D., Michibata, T., Suzuki, K., Takemura, T., Tomita, H. and Nakajima, T.: Aerosol effects on cloud water
575   amounts were successfully simulated by a global cloud-system resolving model, Nature Communications, 9(1),
doi:10.1038/s41467-018-03379-6, 2018.

Sato, Y. and Suzuki, K.: How do aerosols affect cloudiness?, Science, 363(6427), 580–581, doi:10.1126/science.aaw3720,
2019.

Satoh, M., Matsuno, T., Tomita, H., Miura, H., Nasuno, T. and Iga, S.: Nonhydrostatic icosahedral atmospheric model
580   (NICAM) for global cloud resolving simulations, Journal of Computational Physics, 227(7), 3486–3514,
doi:10.1016/j.jcp.2007.02.006, 2008.

Satoh, M., Tomita, H., Miura, H., Iga, S. and Nasuno, T.: Development of a global cloud resolving model – a multi-scale
structure of tropical convections –, , 3, 9, 2005.

Satoh, M., Tomita, H., Yashiro, H., Miura, H., Kodama, C., Seiki, T., Noda, A. T., Yamada, Y., Goto, D., Sawada, M.,
585   Miyoshi, T., Niwa, Y., Hara, M., Ohno, T., Iga, S., Arakawa, T., Inoue, T. and Kubokawa, H.: The Non-hydrostatic
Icosahedral Atmospheric Model: description and development, Prog. in Earth and Planet. Sci., 1(1), 18, doi:10.1186/s40645-
014-0018-1, 2014.

Sayer, A. M., Munchak, L. A., Hsu, N. C., Levy, R. C., Bettenhausen, C. and Jeong, M.-J.: MODIS Collection 6 aerosol
products: Comparison between Aqua's e-Deep Blue, Dark Target, and "merged" data sets, and usage recommendations,
590   Journal of Geophysical Research: Atmospheres, 119(24), 13,965-13,989, doi:10.1002/2014JD022453, 2014.

Schuster, G. L., Vaughan, M., MacDonnell, D., Su, W., Winker, D., Dubovik, O., Lapyonok, T. and Trepte, C.: Comparison
of CALIPSO aerosol optical depth retrievals to AERONET measurements, and a climatology for the lidar ratio of dust,
Atmos. Chem. Phys., 12(16), 7431–7452, doi:10.5194/acp-12-7431-2012, 2012.

Schutgens, N. A. J., Miyoshi, T., Takemura, T. and Nakajima, T.: Applying an ensemble Kalman filter to the assimilation of
595   AERONET observations in a global aerosol transport model, Atmos. Chem. Phys., 16, 2010a.

Schutgens, N. A. J., Miyoshi, T., Takemura, T. and Nakajima, T.: Sensitivity tests for an ensemble Kalman filter for aerosol
assimilation, Atmos. Chem. Phys., 18, 2010b.

Schutgens, N., Tsyro, S., Gryspeerdt, E., Goto, D., Weigum, N., Schulz, M. and Stier, P.: On the spatio-temporal
representativeness of observations, Atmos. Chem. Phys., 17(16), 9761–9780, doi:10.5194/acp-17-9761-2017, 2017.

600   Sekiyama, T. T., Tanaka, T. Y., Shimizu, A. and Miyoshi, T.: Data assimilation of CALIPSO aerosol observations, Atmos.
Chem. Phys., 11, 2010.

Sorooshian, A. and Duong, H. T.: Ocean Emission Effects on Aerosol-Cloud Interactions: Insights from Two Case Studies,
Advances in Meteorology, 2010, 1–9, doi:10.1155/2010/301395, 2010.

Takemura, T.: Aerosol distributions and radiative forcing over the Asian Pacific region simulated by Spectral Radiation-Transport Model for Aerosol Species (SPRINTARS), Journal of Geophysical Research, 108(D23), 8659, doi:10.1029/2002JD003210, 2003.

Takemura, T., Egashira, M., Matsuzawa, K., Ichijo, H., O'ishi, R. and Abe-Ouchi, A.: A simulation of the global distribution and radiative forcing of soil dust aerosols at the Last Glacial Maximum, Atmospheric Chemistry and Physics, 9(9), 3061–3073, doi:10.5194/acp-9-3061-2009, 2009.

Takemura, T., Okamoto, H., Maruyama, Y., Numaguti, A., Higurashi, A. and Nakajima, T.: Global three-dimensional simulation of aerosol optical thickness distribution of various origins, J. Geophys. Res., 105(D14), 17853–17873, doi:10.1029/2000JD900265, 2000.

Taylor, K. E.: Summarizing multiple aspects of model performance in a single diagram, J. Geophys. Res., 106(D7), 7183-7192, doi: 10.1029/2000jd900719, 2001.

Textor, C., Schulz, M., Guibert, S., Kinne, S., Balkanski, Y., Bauer, S., Berntsen, T., Berglen, T., Boucher, O., Chin, M., Dentener, F., Diehl, T., Easter, R., Feichter, H., Fillmore, D., Ghan, S., Ginoux, P., Gong, S., Grini, A., Hendricks, J., Horowitz, L., Huang, P., Isaksen, I., Iversen, T., Kloster, S., Koch, D., Kirkeva, A., Kristjansson, J. E., Krol, M., Lauer, A., Lamarque, J. F., Liu, X., Montanaro, V., Myhre, G., Penner, J., Pitari, G., Reddy, S., Seland, Ø., Stier, P., Takemura, T. and Tie, X.: Analysis and quantification of the diversities of aerosol life cycles within AeroCom, Atmos. Chem. Phys., 37, 2006.

Tomita, H. and Satoh, M.: A new dynamical framework of nonhydrostatic global model using the icosahedral grid, Fluid Dynamics Research, 44, 2004.

Uchida, J., Mori, M., Nakamura, H., Satoh, M., Suzuki, K. and Nakajima, T.: Error and Energy Budget Analysis of a Nonhydrostatic Stretched-Grid Global Atmospheric Model, Monthly Weather Review, 144(4), 1423–1447, doi:10.1175/MWR-D-15-0271.1, 2016.

Uchida, J., Mori, M., Hara, M., Satoh, M., Goto, D., Kataoka, T., Suzuki, K. and Nakajima, T.: Impact of Lateral Boundary Errors on the Simulation of Clouds with a Nonhydrostatic Regional Climate Model, Monthly Weather Review, 145(12), 5059–5082, doi:10.1175/MWR-D-17-0158.1, 2017.

Uno, I., Yumimoto, K., Shimizu, A., Hara, Y., Sugimoto, N., Wang, Z., Liu, Z. and Winker, D. M.: 3D structure of Asian dust transport revealed by CALIPSO lidar and a 4DVAR dust model, Geophysical Research Letters, 35(6), doi:10.1029/2007GL032329, 2008.

van der Werf, G. R., Randerson, J. T., Giglio, L., Collatz, G. J., Mu, M., Kasibhatla, P. S., Morton, D. C., DeFries, R. S., Jin, Y. and van Leeuwen, T. T.: Global fire emissions and the contribution of deforestation, savanna, forest, agricultural, and peat fires (1997–2009), Atmos. Chem. Phys., 10(23), 11707–11735, doi:10.5194/acp-10-11707-2010, 2010.

Watson-Parris, D., Schutgens, N., Cook, N., Kipling, Z., Kershaw, P., Gryspeerdt, E., Lawrence, B. and Stier, P.:
635   Community Intercomparison Suite (CIS) v1.4.0: a tool for intercomparing models and observations, Geoscientific Model
Development, 9(9), 3093–3110, doi:10.5194/gmd-9-3093-2016, 2016.

Willmott, C. J., Robeson, S. M., and Matsuura, K.: A refined index of model performance, International Journal of
Climatology, 32, 2088-2094, 10.1002/joc.2419, 2012.

Winker, D. M., Hunt, W. H. and McGill, M. J.: Initial performance assessment of CALIOP, Geophysical Research Letters,
640   34(19), doi:10.1029/2007GL030135, 2007.

Yin, X., Dai, T., Schutgens, N. A. J., Goto, D., Nakajima, T. and Shi, G.: Effects of data assimilation on the global aerosol
key optical properties simulations, Atmospheric Research, 178–179, 175–186, doi:10.1016/j.atmosres.2016.03.016, 2016a.

Yin, X.-M., Dai, T., Xin, J.-Y., Gong, D.-Y., Yang, J., Teruyuki, N. and Shi, G.-Y.: Estimation of aerosol properties over the
Chinese desert region with MODIS AOD assimilation in a global model, Advances in Climate Change Research, 7(1–2), 90–
645   98, doi:10.1016/j.accre.2016.04.001, 2016b.

Young, S. A. and Vaughan, M. A.: The Retrieval of Profiles of Particulate Extinction from Cloud-Aerosol Lidar Infrared
Pathfinder Satellite Observations (CALIPSO) Data: Algorithm Description, Journal of Atmospheric and Oceanic
Technology, 26(6), 1105–1119, doi:10.1175/2008JTECHA1221.1, 2009.

Yu, H., Chin, M., Winker, D. M., Omar, A. H., Liu, Z., Kittaka, C. and Diehl, T.: Global view of aerosol vertical
650   distributions from CALIPSO lidar measurements and GOCART simulations: Regional and seasonal variations, Journal of
Geophysical Research, 115, doi:10.1029/2009JD013364, 2010.

Yumimoto, K. and Takemura, T.: Direct radiative effect of aerosols estimated using ensemble-based data assimilation in a
global aerosol climate model: ASSIMILATION WITH AEROSOL CLIMATE MODEL, Geophysical Research Letters,
38(21), doi:10.1029/2011GL049258, 2011.

655   Yumimoto, K., Tanaka, T. Y., Oshima, N. and Maki, T.: JRAero: the Japanese Reanalysis for Aerosol v1.0, Geosci. Model
Dev., 29, 2017.

Yumimoto, K., Tanaka, T. Y., Yoshida, M., Kikuchi, M., Nagao, T. M., Murakami, H. and Maki, T.: Assimilation and
Forecasting Experiment for Heavy Siberian Wildfire Smoke in May 2016 with Himawari-8 Aerosol Optical Thickness,
Journal of the Meteorological Society of Japan. Ser. II, 96B(0), 133–149, doi:10.2151/jmsj.2018-035, 2018.

660   Yumimoto, K., Uno, I., Sugimoto, N., Shimizu, A., Liu, Z. and Winker, D. M.: Adjoint inversion modeling of Asian dust
emission using lidar observations, Atmospheric Chemistry and Physics, 8(11), 2869–2884, doi:10.5194/acp-8-2869-2008,
2008.

Zhang, J. and Reid, J. S.: MODIS aerosol product analysis for data assimilation: Assessment of over-ocean level 2 aerosol optical thickness retrievals, Journal of Geophysical Research, 111(D22), doi:10.1029/2005JD006898, 2006.

665 Zhang, J., Campbell, J. R., Reid, J. S., Westphal, D. L., Baker, N. L., Campbell, W. F. and Hyer, E. J.: Evaluating the impact of assimilating CALIOP-derived aerosol extinction profiles on a global mass transport model: CALIOP DATA ASSIMILATION, Geophysical Research Letters, 38(L14801), doi:10.1029/2011GL047737, 2011.

Zhang, J., Campbell, J. R., Hyer, E. J., Reid, J. S., Westphal, D. L. and Johnson, R. S.: Evaluating the impact of multisensor data assimilation on a global aerosol particle transport model: Multi-Sensor Aerosol Data Assimilation, Journal of

670 Geophysical Research: Atmospheres, 119(8), 4674–4689, doi:10.1002/2013JD020975, 2014.
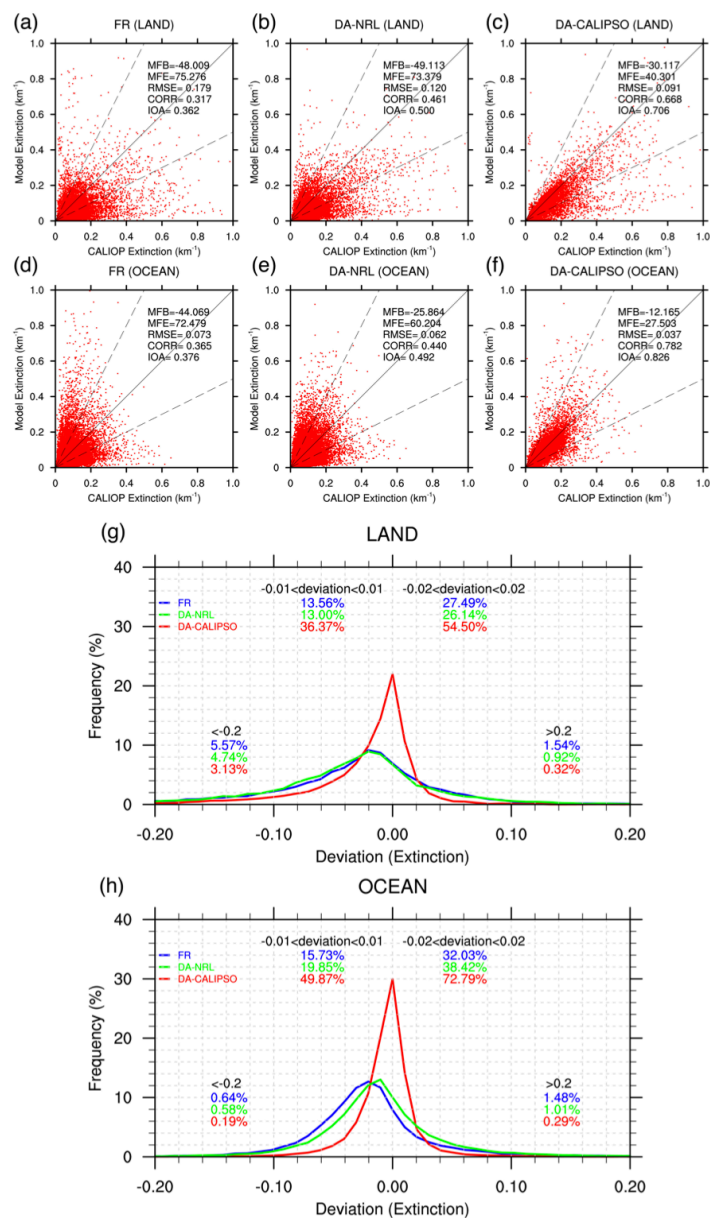
Figure 1. Scatter plots of the CALIOP (Cloud-Aerosol Lidar with Orthogonal Polarization) hourly aerosol extinction coefficients at 532 nm [km⁻¹] versus the simulated ones at 550 nm over the global land (a, b, c) and ocean (d, e, f) during November 2016 for the FR, DA-NRL, and DA-CALIPSO experiments. The solid black line is the 1:1 line and the dashed black lines correspond to the 1:2 and 2:1 lines. MFB, MFE, RMSE, CORR, and IOA represent the mean fractional bias, the mean fractional error, the root mean square error, the correlation coefficient and the index of agreement, respectively. Frequency distributions of deviations (modeled extinction coefficients minus the CALIOP observed ones) over the global land (g) and ocean (h). The percentages of deviations between ±0.01, ±0.02, <-0.2 and >0.2 are also shown.
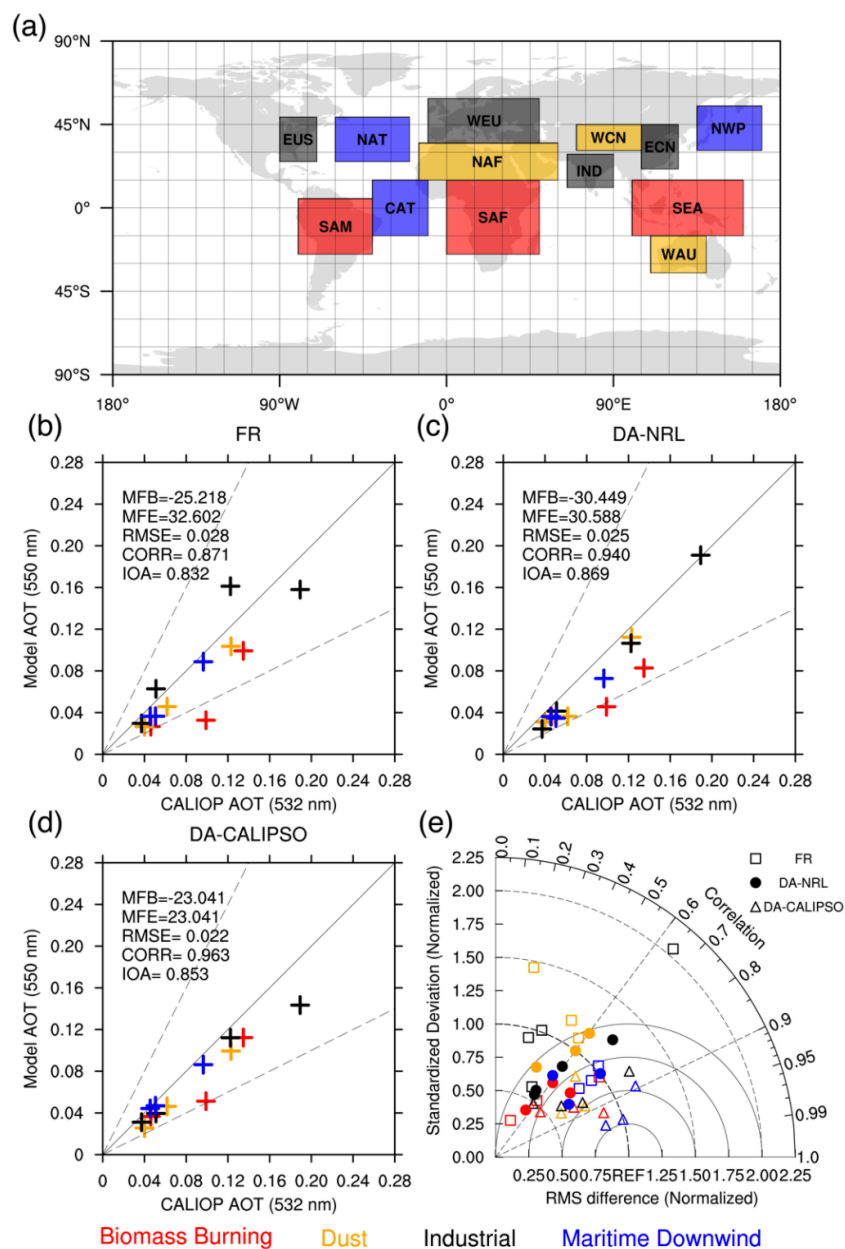
Figure 2. (a) Thirteen domains selected for regional analysis in this study. The red, orange, black and blue boxes indicate source regions of biomass burning smoke (SAM, SAF, and SEA), dust (NAF, WCN, and WAU), industrial pollution (IND, ECN, WEU, and EUS), and the outflow maritime regions downwind of major dust and industrial pollution sources (NWP, NAT, and CAT), respectively. Scatter plots of the simulated regionally averaged monthly mean column-integrated aerosol extinctions at 550 nm versus the collocated CALIOP ones at 532 nm over the thirteen selected regions during November 2016 for the FR (b), DA-NRL (c), and DA-CALIPSO (d) experiments. (e) The Taylor graph describing the column-integrated aerosol extinctions in the three experiments compared with the observed ones.
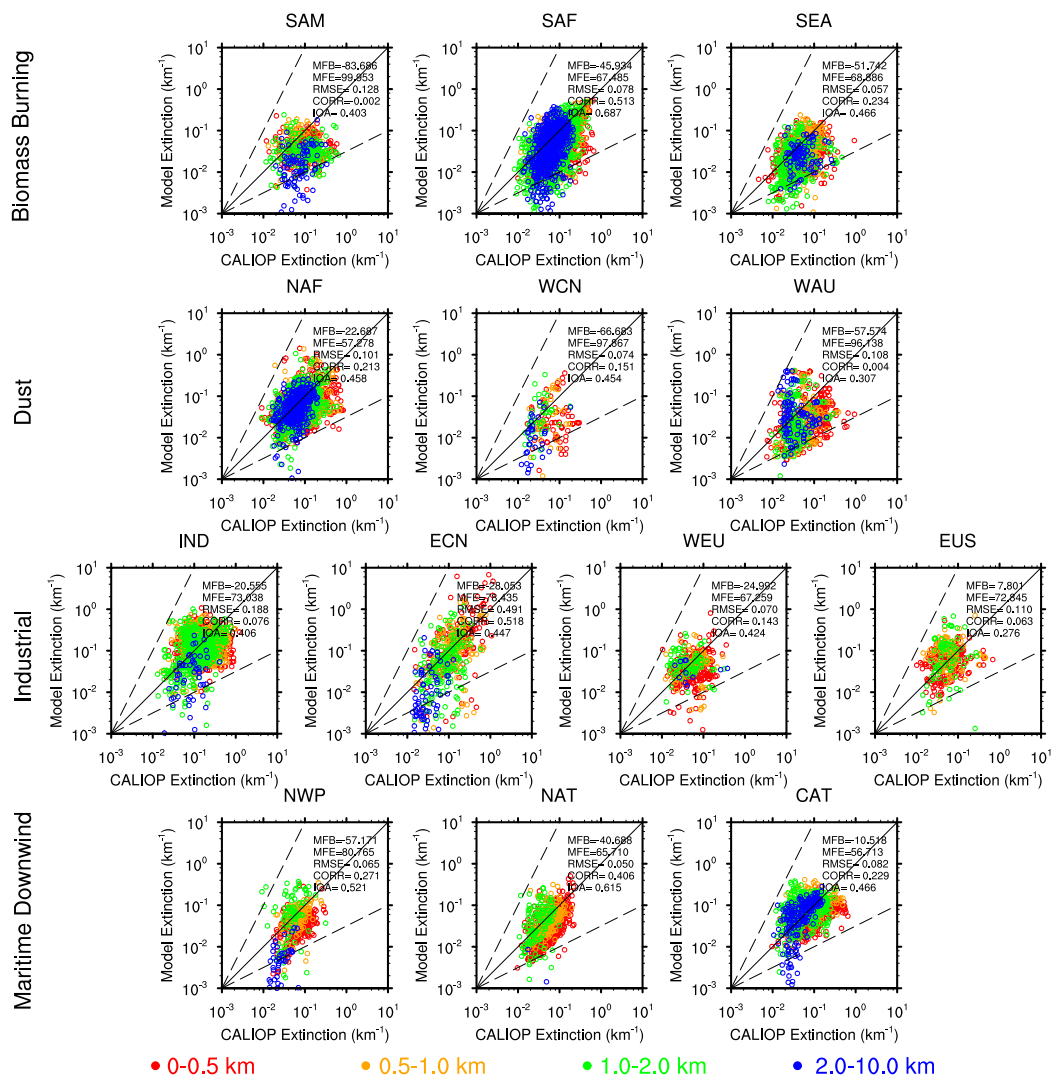
Figure 3. Scatter plots of the FR experiment simulated hourly aerosol extinction coefficients at 550 nm [km⁻¹] versus the CALIOP observed ones at 532 nm over the thirteen selected regions during November 2016.
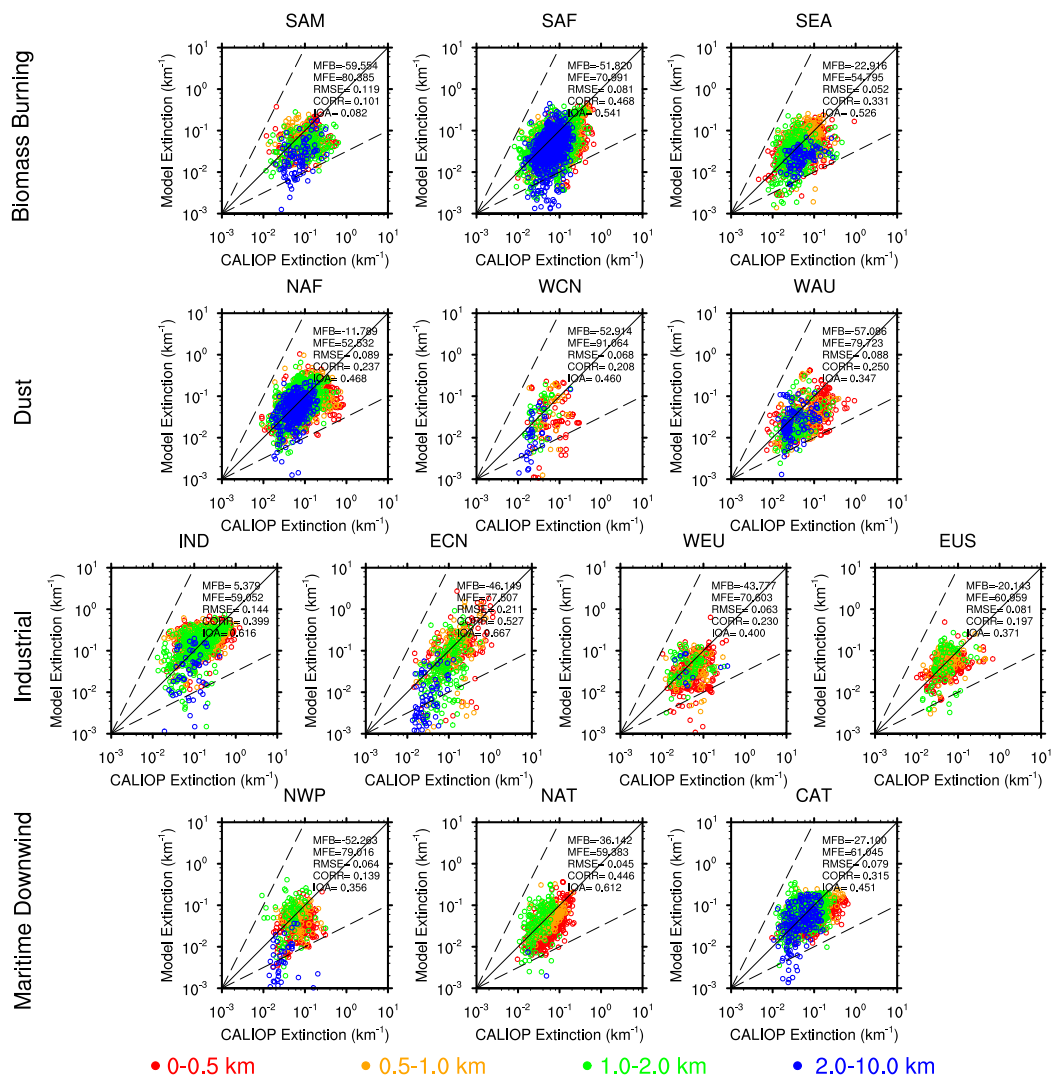
Figure 4. Same as Figure 3 but for the DA-NRL experiment.
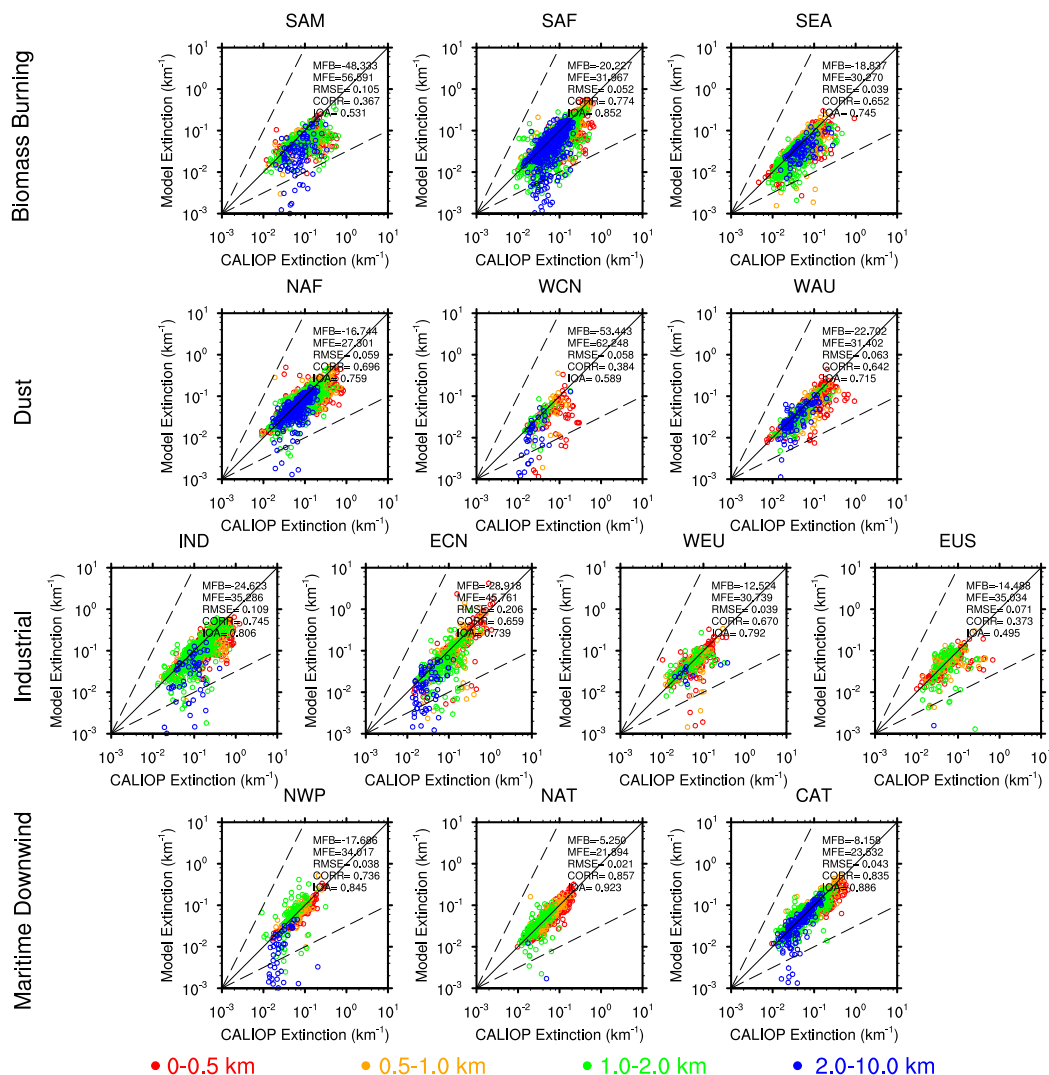
Figure 5. Same as Figure 3 but for the DA-CALIPSO experiment.
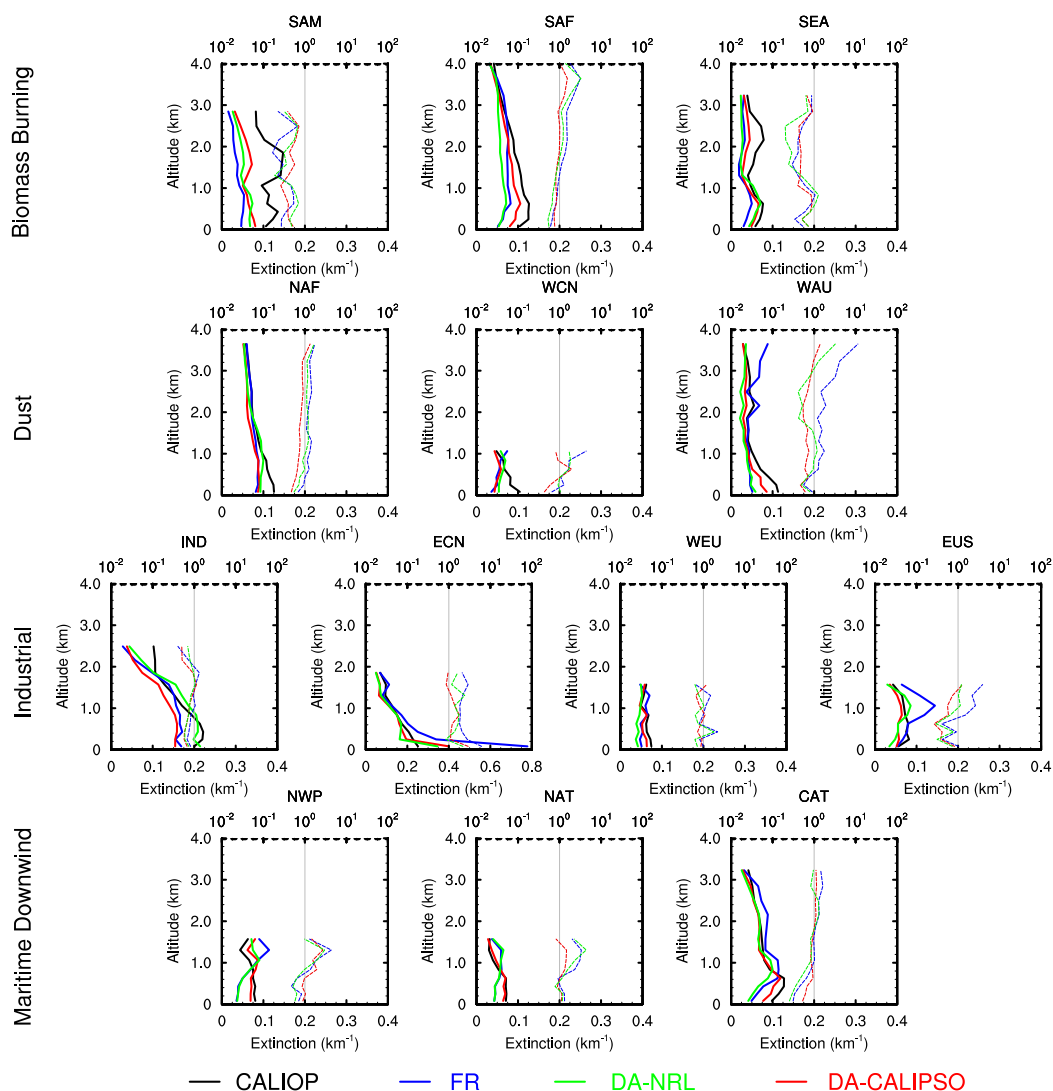
Figure 6. Regionally averaged monthly mean vertical profiles of the three experiments simulated aerosol extinction coefficients at 550 nm [km⁻¹] and the CALIOP observed ones at 532 nm (solid lines) and the ratios between the simulated and observed standard deviations (dashed line) over the thirteen selected regions during November 2016.
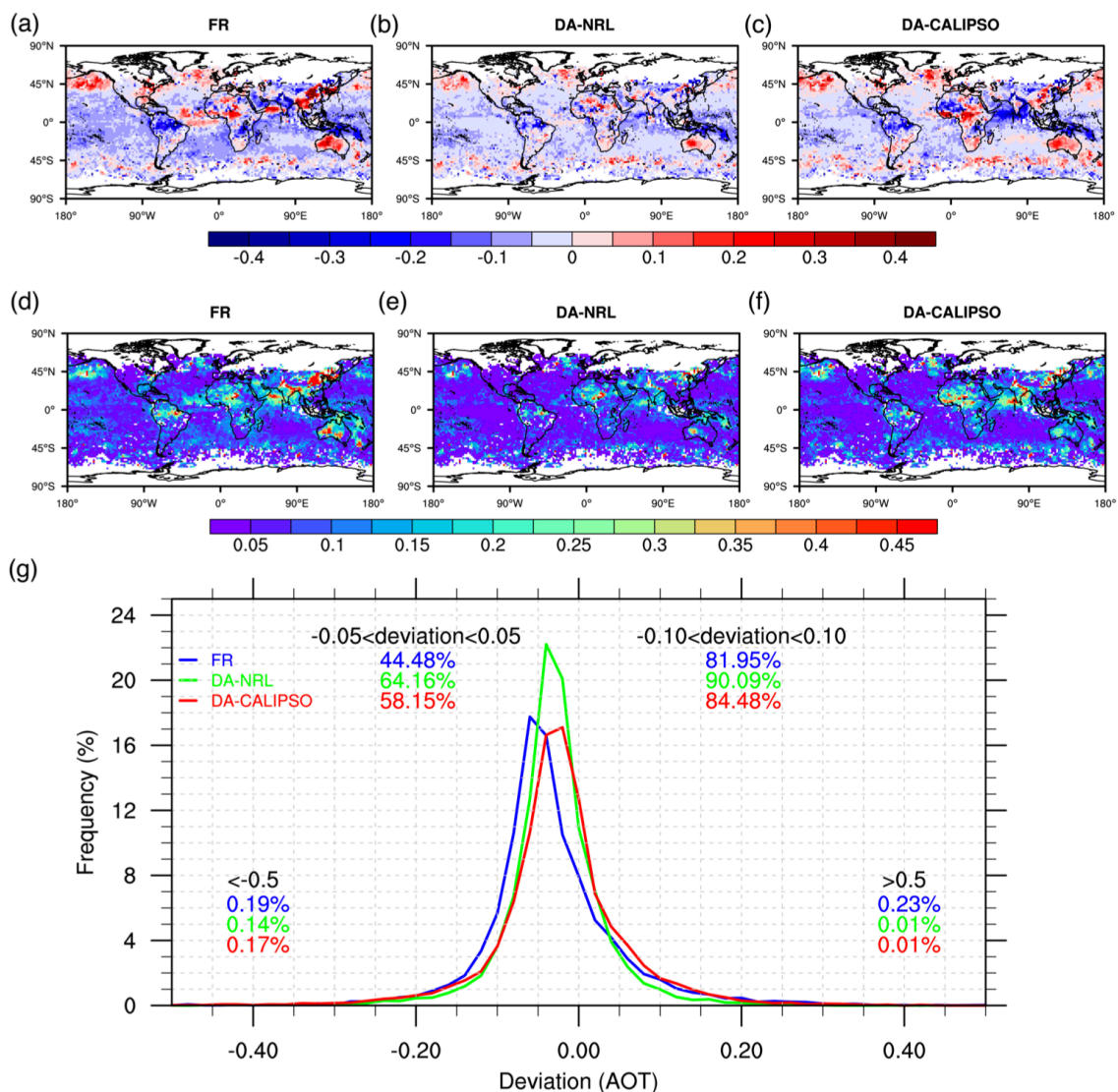
700 **Figure 7. Spatial distributions of the biases (the simulated AOTs minus the observed ones) (a, b, c) and root-mean-square errors (d, e, f) between the simulated and the Moderate Resolution Imaging Spectroradiometer (MODIS) Aqua observed AOTs at 550 nm during November 2016 for the FR, DA-NRL, and DA-CALIPSO experiments. (g) Frequency distributions of deviations (the simulated AOTs minus the observed ones) from the MODIS Aqua observations. The percentages of deviations between ±0.05, ±0.10, <-0.5 and >0.5 are also shown.**
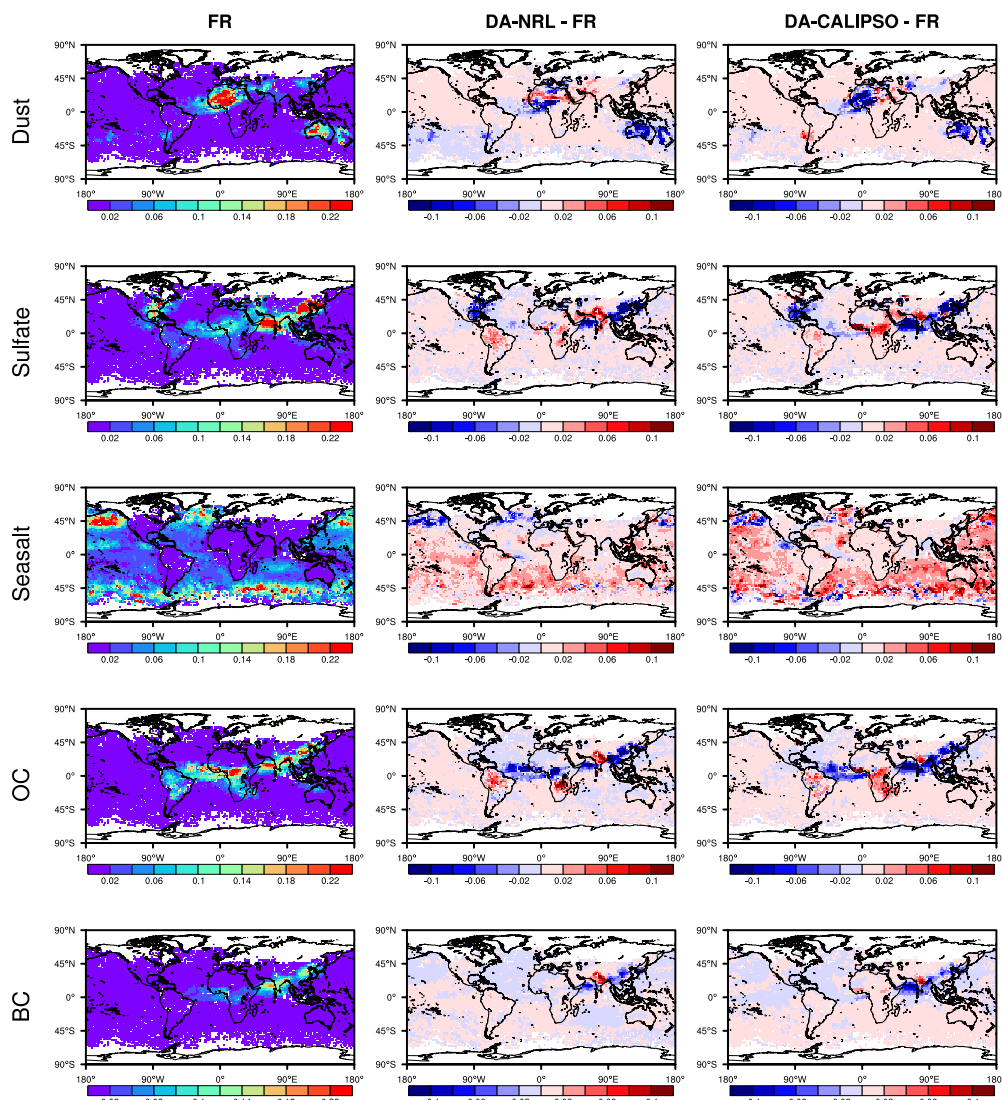
705

Figure 8. Spatial distributions of the monthly mean AOTs at 550 nm in the FR experiment (sampled to the MODIS observations) and the mean differences of the AOTs in the two assimilation experiments (DA-NRL and DA-CALIPSO) minus those in the FR experiment for each individual aerosol component (i.e., dust, sulfate, sea salt, organic carbon [OC], and black carbon [BC]) during November 2016.
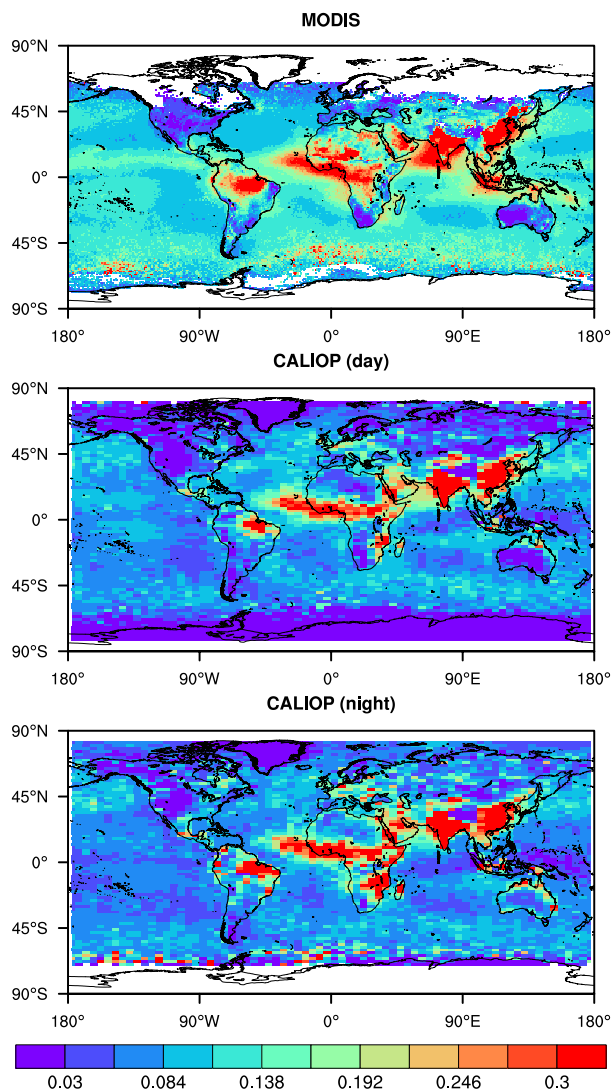
710

Figure 9. Spatial distributions of the monthly mean MODIS Aqua AOTs at 550 nm, day-time CALIOP and night-time CALIOP AOTs at 532 nm in November from 2006 to 2016.
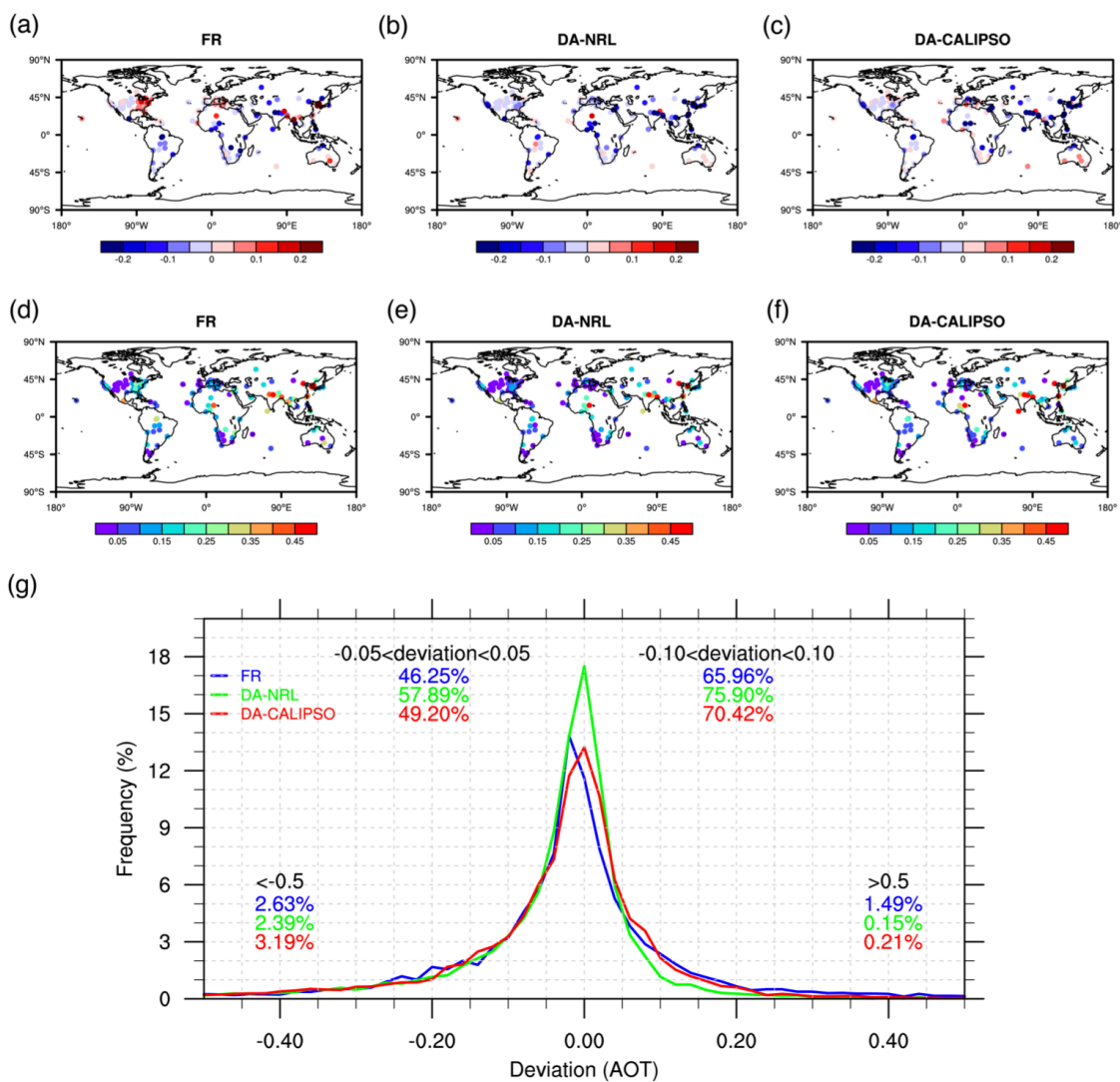
Figure 10. Same as Figure 7 but for the simulated AOTs at 440 nm against the AErosol RObotic NETwork (AERONET)-retrieved ones.
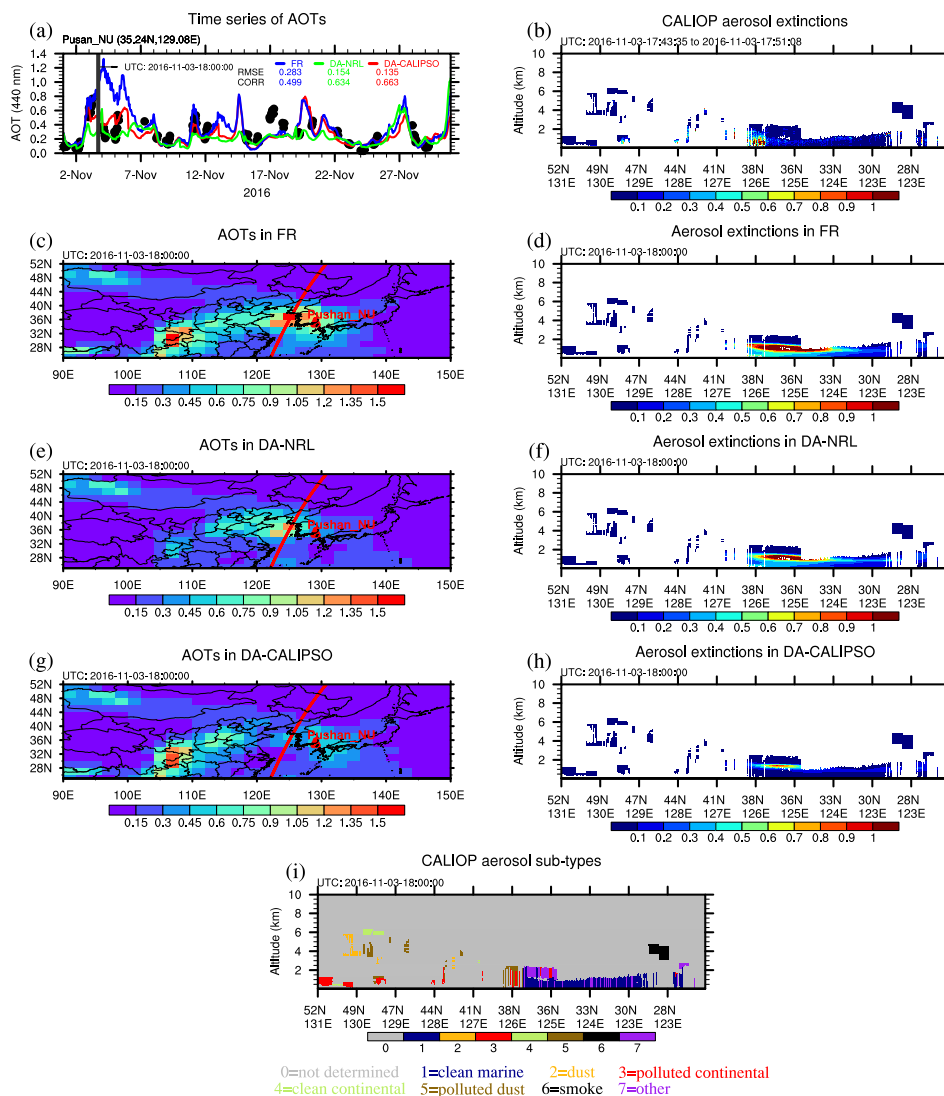
Figure 11. (a) Hourly time series of the AOTs at 440 nm for the FR, DA-NRL, and DA-CALIPSO experiments and the observed AOTs from AErosol RObotic NETwork (AERONET) over Pushan_NU site during November 2016. The root-mean-square error (RMSE) and correlation coefficient (CORR) between the simulated and the observed AOTs are also shown. The spatial distributions of the simulated AOTs at 440 nm at 18:00:00 (UTC) 3 November 2016 in the FR (c), DA-NRL (e), and DA-CALIPSO (g) experiments. The red triangle indicates the location of Pushan_NU site. The red curve indicates one CALIPSO orbit path near the Pushan_NU site on 3 November 2016. The CALIOP observed aerosol extinction coefficients at 532 nm [km^{-1}] (b) and the simulated ones at 550 nm in the FR (d), DA-NRL (f), and DA-CALIPSO (h) experiments over that CALIPSO orbit path. (g) CALIPSO derived vertical aerosol sub-types.

720
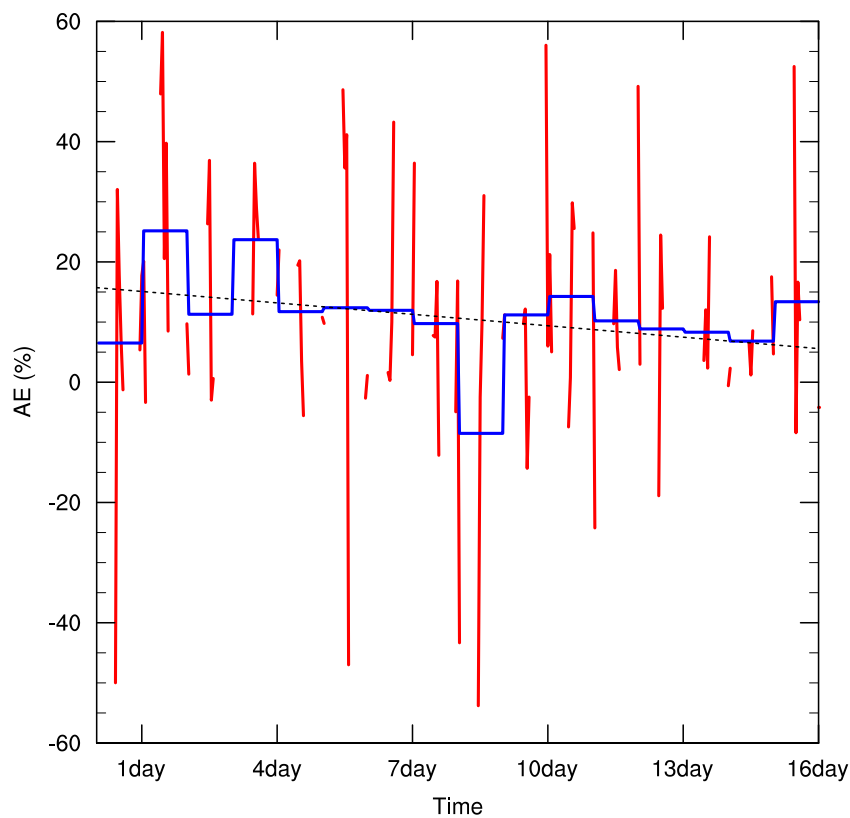
725

Figure 12. Assimilation efficiencies (AE) calculated against the Moderate Resolution Imaging Spectroradiometer (MODIS) Aqua observed AOTs at 550 nm for the DA-CALIPSO experiment as the function of the distance of the assimilation time. The daily mean time series and the linear regression line are shown as the blue solid and the black dashed lines, respectively.
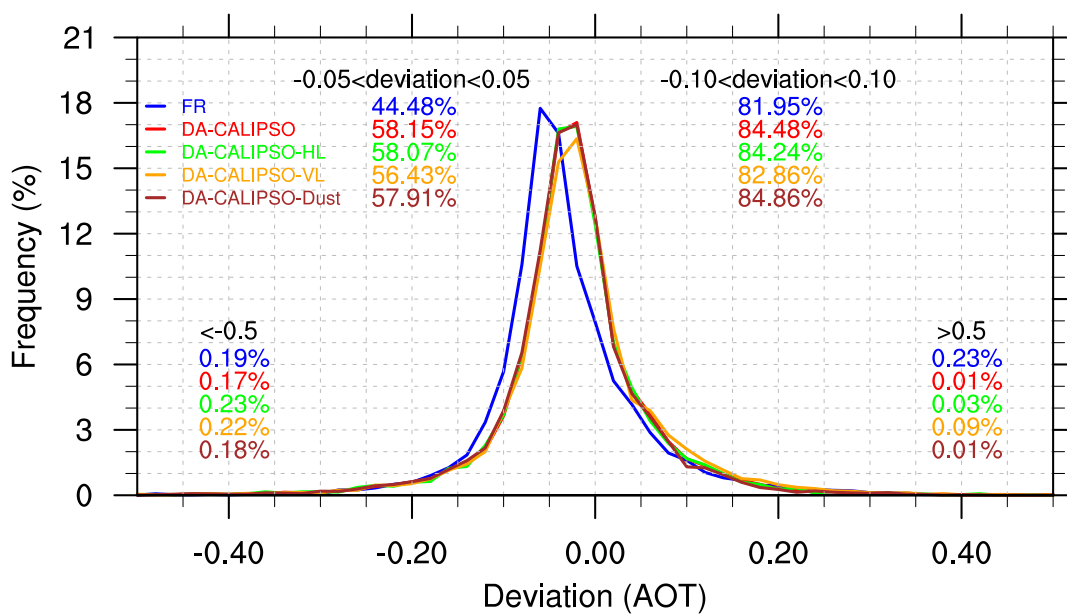
Figure 13. Frequency distributions of deviations (the simulated AOTs minus the observed AOTs) from the Moderate Resolution Imaging Spectroradiometer (MODIS) Aqua observed AOTs at 550 nm for the FR, DA-CALIPSO, DA-CALIPSO-HL, DA-CALIPSO-VL, and DA-CALIPSO-Dust experiments. The percentages of deviations between ±0.05, ±0.10, <-0.5 and >0.5 are also shown.